IS-T-869

SINGLE CRYSTAL LaB_6

Max Arnold Noack

M.S. Thesis Submitted to Iowa State University

Ames Laboratory, USDOE
Iowa State University
Ames, Iowa 50011

Date Transmitted: July 1979

PREPARED FOR THE U.S. DEPARTMENT OF ENERGY
UNDER CONTRACT NO. W-7405-eng-82

DISCLAIMER

NOTICE

Available from: National Technical Information Service
U. S. Department of Commerce
P.O. Box 1553
Springfield, VA 22161

Price: Microfiche $3.00

Single crystal LaB_6

by

Max Arnold Noack

A Thesis Submitted to the

Graduate Faculty in Partial Fulfillment of

The Requirements for the Degree of

MASTER OF SCIENCE

Department: Materials Science and Engineering
Major: Metallurgy

Approved:

John Verhoeven
In Charge of Major Work

For the Major Department

For the Graduate College

Iowa State University
Ames, Iowa

1979

TABLE OF CONTENTS

Single Crystal LaB_6

by

Max Arnold Noack

ABSTRACT

Single crystals of LaB_6 were prepared by float zone refining of hot pressed blocks of LaB_6. The orientations studied were (001), (110), and a high index plane. The resulting crystals and the as-received material were chemically analyzed by the following techniques: vacuum fusion, combustion analysis, self-arc mass spectroscopy, and wet chemical analysis. The first two techniques provided accurate analysis for O, N, H, and C. The remaining elements except for La and B were determined by mass spectroscopy. The wet chemical analyses determined the B/La ratio. Two batches of as-received material had B/La ratios of 6.0 and 5.8, respectively. Slightly lower B/La ratios were obtained in the single crystals grown by the float zone technique from these materials. The single crystals were further characterized by measurements of lattice parameter and density.

The work function values were determined by the FERP method and the thermionic method. The work function measurements in conjunction with Auger analysis of these crystals provided insight into the electron emission character of LaB_6. These results indicate that for maximum emission from a crystal plane a proper heat treatment is necessary.

The brightness of these crystals was measured in a Cambridge S-4 scanning electron microscope using a Broers type gun. The results show that a brightness of 10^6 amp/cm^2 steradian (20kV) may be achieved with a single crystal LaB_6 cathode operating at a temperature of 1900^{o}K which corresponds to a lifetime greater than 500 hrs. for 1 mm cathodes.

INTRODUCTION

It is recognized that the performance of most electron beam instruments is limited by the brightness of the electron source. The brightness of the source determines the maximum current available for a focused beam diameter of a given divergence angle given by the following relationship.

$$I = B\pi^2 d^2 \alpha^2 / C \qquad (1)$$

where I = beam current

B = beam brightness

π = pi, a constant

d = beam diameter

α = beam divergence half angle

C = a constant

The brightness of a source is the current density per unit solid angle (amp/cm^2 · steradian) supplied by the emitter. The brightness of thermal cathode electron guns is given by the following relationship which can be derived from the work of Langmuir (1).

$$B = \frac{J_c}{\pi}\left(1 + \frac{eV}{\kappa T}\right) \simeq \frac{J_c}{\pi}\ \frac{11{,}605\ V}{T} \qquad (2)$$

where J_c = specific emission of the cathode

e = electron charge

V = accelerating potential

κ = Boltzmann's constant

T = absolute temperature of the cathode

The cathode current density, J_c, can be increased by an increase of the cathode temperature according to the well-known Richardson-Laue-Dushmann equation.

$$J_c = AT^2 (1-\bar{r}) \exp (-e\phi/\kappa T) \qquad (3)$$

where A = universal thermionic constant

T = absolute temperature of cathode

$\bar{r}$ = reflection coefficient

e = electron charge

ϕ = work function of cathode

κ = Boltzmann's constant

However, as the temperature is increased, the lifetime of the cathode becomes severely limited. The most widely used source, the tungsten thermionic filament, has a cathode current density of about $1A/cm^2$ for an acceptable lifetime of 30 hours.

The most promising approach to simultaneously improving the brightness and lifetime is the use of thermionic emitters with a lower work function than tungsten. Lafferty (2) investigated several materials and recommended lanthanum hexaboride, LaB_6, as a high brightness electron emitter in 1951. He showed that higher ratios of electron emission density to evaporation rate exist for LaB_6 than for tungsten, and that

the electron emission from LaB_6 is maintained under the usual vacuum conditions ($\sim 10^{-6}$ mmHg) found in demountable vacuum systems. Shortly thereafter, many investigations of LaB_6 were reported. Heemstra (3) and later Decker and Stebbins (4) measured the work function of LaB_6 at Ames Laboratory, Ames, Iowa. The lanthanum-boron phase diagram was also determined there (5). Bertaut and Blum (6) measured the lattice parameter of LaB_6 prepared by electrolysis of a fused salt bath. Post et al. (7) measured the lattice parameter of LaB_6 prepared by reduction of lanthanum oxide with boron powder. However, the use of LaB_6 as a cathode material in electron guns did not follow immediately.

Because LaB_6 is a brittle material and quite chemically reactive at the temperature of interest, it requires an electron gun design different from the conventional tungsten electron gun for its utilization. The use of LaB_6 as a cathode material was initiated primarily by the Broers' gun design in 1967 (8). Subsequent evaluation of LaB_6 as a cathode in an electron gun revealed improvements with respect to the tungsten hairpin cathode as regards brightness and cathode life (8,9,10,11).

However, there was disagreement among investigators about the maximum brightness to be expected from LaB_6 (12,13). This was a result of the uncertainty in the knowledge of the specific emission of the LaB_6 cathode. In the Handbook of Thermionic Properties by V. S. Fomenko (14), the effective work functions listed range from

2.7 to 3.2 eV. Investigators even disagreed about the effect of varying the boron to lanthanum composition. In High-Temperature Compounds of Rare Earth Metals with Nonmetals, Samsonov (15) reports a work function of 2.16 eV for LaB_6 with an effective composition LaB_{12}. This would imply an increase in boron content lowered the work function. However, Ermakov et al. (16) observed the opposite effect. For a given purity of LaB_6, they reported an increase in work function with an increase in the boron content.

It was thought that the disagreements and the large scatter of the reported data were a result of using sintered LaB_6 materials in these investigations. The absence of large enough pieces of single crystal LaB_6 to make complete cathodes was attributed by Broers' (17) as a major reason for the difficulty in obtaining the maximum brightness. He reported "lobes" of high electron emission were obtained with sintered material.

The purpose of this investigation was to provide data on the electron emission of LaB_6. These data could then provide reliable information for obtaining the maximum performance of LaB_6 as an electron emitter. For this information to be reliable, it was thought that the measurements would need to be done on carefully characterized single crystal material.

This project was conducted in four parts. First, single crystals of LaB_6 that were large enough to make complete cathodes were produced. Second, these crystals were characterized by purity, boron and

lanthanum composition, melting point, density, lattice parameter, and crystallographic orientation. Then, the brightness and lifetimes were evaluated in an electron gun similar to Broers' design. Lastly, the specific emission of the single crystal LaB_6 was measured[1].

---

[1]A cooperative arrangement with Dr. L. Swanson of Oregon Graduate Center, Beaverton, Oregon, provided these measurements.

EXPERIMENTAL WORK

A Float Zone Refining Technique

For refractory materials, float zone melting has been shown to be a successful process for producing ultra-high purity material (18). In this process, the melted portion of a rod is held in place only by its own surface tension, thereby avoiding contamination by a crucible container. The small molten zone is passed along a vertical rod. Very slow solidification rates can be achieved by controlling the traverse rate of the molten zone along the rod. Single crystals are likely to result from the slow solidification rate.

The method of heating to produce the molten zone varies. If the material has a low vapor pressure at the melting point, electron bombardment heating can be used. However, the high vapor pressure of LaB_6 excluded this method. Another common method of heating uses rf induced current. This technique was used by others (19,20,21) to produce large diameter rods of boride materials. However, the control of the power output of rf generators is very sluggish. Also, the force of the magnetic field produced by the alternating current has a tendency to pinch the molten zone. Because of these characteristics of the rf induction method, preparation of a rod of suitable uniform diameter was not deemed probable by this method. Laser beam heating and the electric arc were considered to have a sufficient control of their power output to be usable for such small diameter rods. Because of the greater simplicity, lower cost, and availability,

the electric arc was chosen as the method of heating.

Apparatus

The essential components used in this arc float zone technique are illustrated schematically in Figure 1. Stainless steel rods, ¼ inch in diameter, were machined with a longitudinal groove in the ends to hold the starting rods of hot pressed LaB_6. The rods were held in the grooves by a spring loaded tantalum cylinder. This arrangement allowed for thermal expansion of the rods while maintaining the vertical alignment. This was important when initiating successive passes. Otherwise, the thermal stress caused a large jog to result at the molten interface, and this prevented further traverse of the molten zone. The lower rod was attached to a micromanipulator. This allowed rods of different lengths between 20 and 50 mm to be used. The manipulator was also used when necessary to change the size of the molten zone by withdrawing or raising the lower feed rod.

The upper rod holder was attached to a single crystal goniometer. This was used to hold the seed crystal or blank rod. The goniometer was attached to the top of the chamber by means of a threaded screw which matched the locking nut of the goniometer. After attachment, the axis of the goniometer was parallel to the growth axis within 1^{o}. This assembly allowed the seed crystal to be aligned with X-rays using the same goniometer. This procedure eliminated a change of alignment due to a physical transfer. Crystals deviating by as much

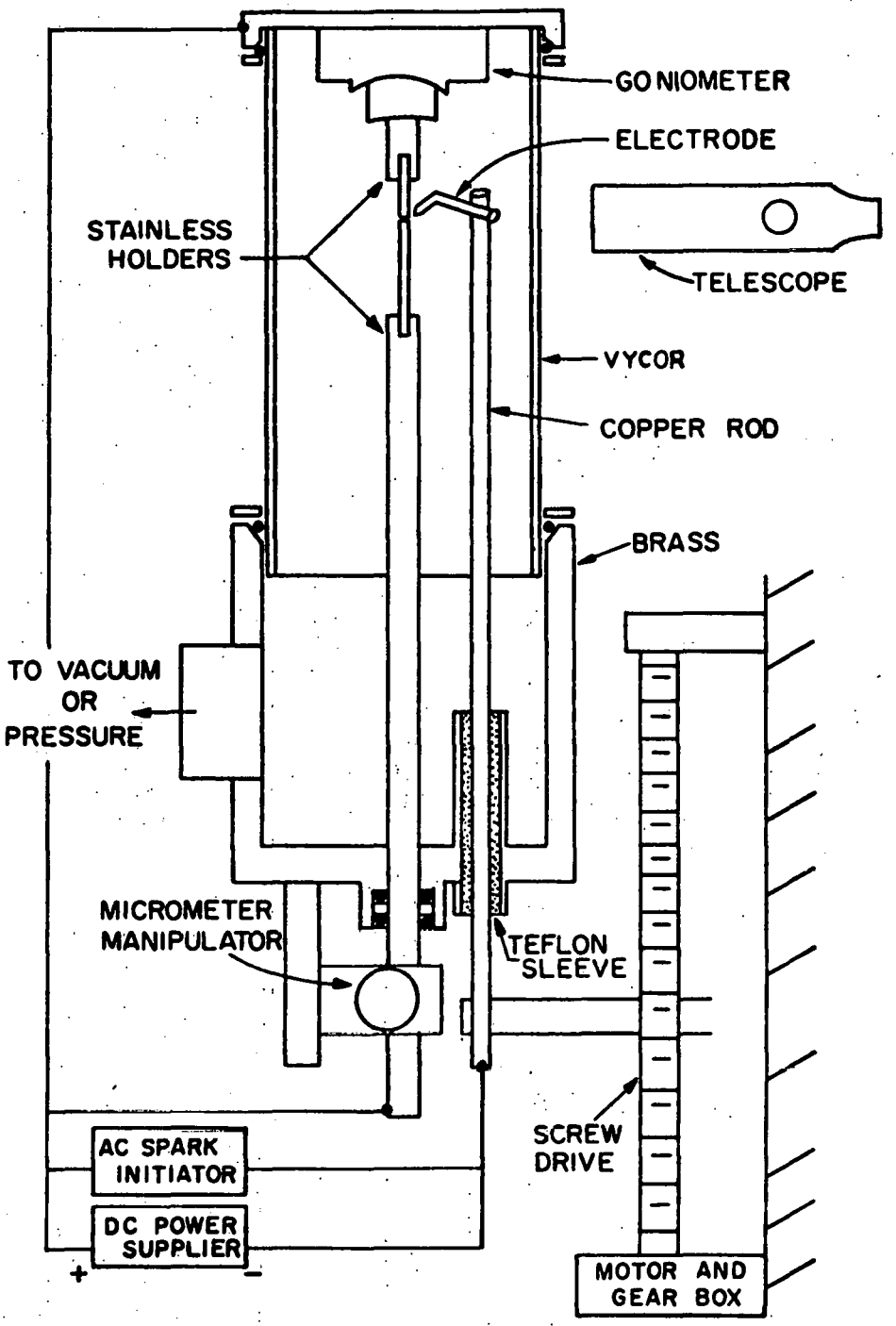

Figure 1. Schematic diagram of apparatus

as 15^{o} from the desired crystal orientation could be used as seed crystals with this arrangement.

Tantalum wire was used exclusively as the electrode material. (Tungsten was also tried, but spark initiation was more easily achieved with tantalum.) A sharp conical point was hand ground on each electrode. The best electrode diameter was between 1.2 and 1.4 mm. Smaller diameter electrodes were found to melt due to the high current. Larger diameter electrodes presented difficulty in establishing an arc. A set-screw was used to hold the electrode in place at the top of a ¼ inch diameter copper rod.

Traverse of the molten zone was achieved by movement of the tantalum electrode. The solidification rate, i.e. the rate of withdrawal of the copper rod, was controlled by the speed of the motor drive mechanism. Travel rates as low as 20 μm/sec were achieved with this arrangement. In all experiments, a travel rate of 50 μm/sec was used.

A small dc welder equipped with an ac spark gap unit was used to initiate the dc arc. Double pole knife switches wired in parallel with the dc welder were used to provide additional current from the constant current dc power supplies. The voltage drop across the arc was around 9 V, but it varied between 8 and 10 V. This variability was caused by the aging of the electrode tip. The current requirements were around 3½, 10, 20, and 40 amps for rods of ½, 1, 1½, and 2 mm diameter, respectively.

Preparation of starting materials

All material used in this work was obtained from Cerac Incorporated, Milwaukee, Wisconsin. The quoted purity, percentage of the X-ray density, and the letter code are given in Table 1. The assigned letter code given each LaB_6 crystal was used to identify the hot pressed block which was the source of the starting blank rods.

Table 1. Hot pressed materials used

Letter code	Cerac lot #	Quote purity	Density
MA	4670	99.9% typ	92%
MB	HP-5154	99.9% min	91%
MC	H-5836	99.9% typ	94.3%
MD	H-6772-A-1c	99.9% typ	91%

The starting blank rods were fabricated by electron discharge machining (EDM) of hot pressed blocks. The EDM uses a dc arc between a copper wire and the sample to volatilize the material. This was done under an oil bath to reduce oxidation and to cool the sample. For cathodes, the starting blanks were cut into 1.04 to 1.07 mm square rods approximately one inch in length. The blanks were ultrasonically cleaned in acetone and freon to degrease them. These blanks were then ground to 1.00 mm square on 100 grit paper. The grinding removed the damaged region caused by EDM, and provided a

uniform cross-section for float zone refining. The blanks were given a final degreasing ultrasonically in solutions of acetone, freon, and finally methyl alcohol. Just before a blank was to be used in the zone melter, it was electropolished for one minute to remove any surface contamination. The electropolish solution of 10 ml of perchloric acid in 225 ml of methanol was cooled to between -60 and -65°C prior to use. A stainless steel beaker was used as the cathode with 30 to 35 V dc applied between it and the LaB_6 blank.

Starting seed crystals were obtained from the zone melting of two blank rods. The seed crystal was oriented using a back-reflection Laue camera. The X-ray beam was parallel to the goniometer axis and thus the growth axis. Alignment of the seed crystal was obtained with a precision of $\pm \frac{1}{2}^{o}$.

Growth of single crystal rod

The goniometer with the seed crystal and blank rod were placed inside the chamber of the zone melter. Viton O-rings provided vacuum and pressure seals. The chamber was evacuated to a pressure of 2×10^{-6} to 5×10^{-6} mmHg with a baffled oil diffusion pump. The chamber was then backfilled with argon to a positive gauge pressure of 12 psi. Argon of two purity levels was used, commercial and ultra zero. The positive pressure of argon was helpful in reducing the vaporization loss of LaB_6. A significant weight loss was measured, and the inside of the chamber was coated with a blue-purple deposit. The deposit was later confirmed by a powder pattern to be LaB_6.

The growth process was carried out as follows. The electrode was moved into position by engaging the motor drive until the electrode was opposite the top of the lower blank rod. The gap between the electrode and the rod was adjusted by rotation of the copper rod holding the electrode. After a gap of approximately 0.2 mm was set, the ac spark initiator was turned on to obtain an electric arc. Then the dc welder was turned on to obtain a dc arc between the electrode and blank rod. Establishment of the dc arc was confirmed by a sudden increase in temperature. The ac spark initiator could then be turned off. The arc gap was increased to approximately 1 mm. Otherwise, the pressure of the arc would push the molten zone so far off axis that the multiple zone passes were impossible.

A traveling telescope, with a darkened glass shield covering the front, was used to observe the arc and rods. The current was increased gradually, switching in power supplies as required, until a molten zone was established between the blank and the seed crystal across the whole diameter. The zone could be observed in the telescope due to a change in emissivity between liquid and solid. The liquid appeared brighter. Once the molten zone was established, it was moved slightly upward into the seed crystal and then traversed downward by engagement of the motor drive mechanism.

The molten zone was continuously observed with the telescope during its passage. Minor adjustments in the molten zone were made during the passage of the zone based on experience of previous

observations. Adjustment of the molten zone could be achieved with either current control of the dc arc, or by the movement of the lower blank rods. The movement of the lower blank rod usually resulted in a non-uniform diameter. So, only the initial adjustment of the molten zone was done with the lower feed rod. Thereafter, during the zone traverse, adjustment was done with the current control. If the proper conditions were used, no adjustments were necessary during the passage of the molten zone. Under these conditions, crystal rods 20 mm and longer in length, having a constant diameter $\pm$ 0.02 mm, were produced.

The most frequent cause for failure of a zone passage was the use of excessive current. Very small changes, 0.1 amps for 1 mm diameter rods, caused significant changes in the diameter and length of the molten zone. A 3% excess current in the arc usually resulted in a catastrophic failure of the molten zone into two separate zones. With experience, the proper current setting to produce a uniform diameter was found.

At the completion of the zone traverse, the motor drive was disengaged and the dc current gradually reduced until the arc extinguished. The successive zone passes were made by repeating the growth process. For multiple passed rods, an additional requirement was discovered. The molten zone had to be stopped slightly above the final zone of the previous pass. Otherwise, the melting point of this region, decreased by the change in concentration, was reduced sufficiently to cause a catastrophic increase in zone length as this

region was approached.

Successive zone passes were observed to accentuate any change in rod diameter. A suitable crystal which was zone passed six times was achieved only after several attempts. Crystal rods of three zone passes, having a uniform diameter, were achieved with reasonable success. It was judged that three zone passes provided sufficient purification to warrant further passes as unnecessary. (See chemical analysis in Results section.)

Examination and Preparation of Single Crystal Rods

After completion of zone pass or passes, the rod was allowed to cool to room temperature. Upon opening the zone melter chamber, a pungent odor was always noted. The seed crystal and zone refined rod were removed intact. The rod was sectioned as necessary by EDM or by a slow speed diamond saw. The diamond saw was used exclusively to obtain sections for work function measurements. The top of the crystal rod was mechanically polished transversely with 600 grit SiC paper and electropolished smooth using the perchloric solution. This presented a suitable surface for crystallographic analysis using the selected area channelling mode of the scanning electron microscope (SEM). This technique provided more and better crystallographic information than available from the Laue technique.

A grinding jig illustrated in Figure 2 was used to prepare the surface of the transverse sections. A low melting wax was used to hold the cylindrical sections in the V-groove. By rotation of the

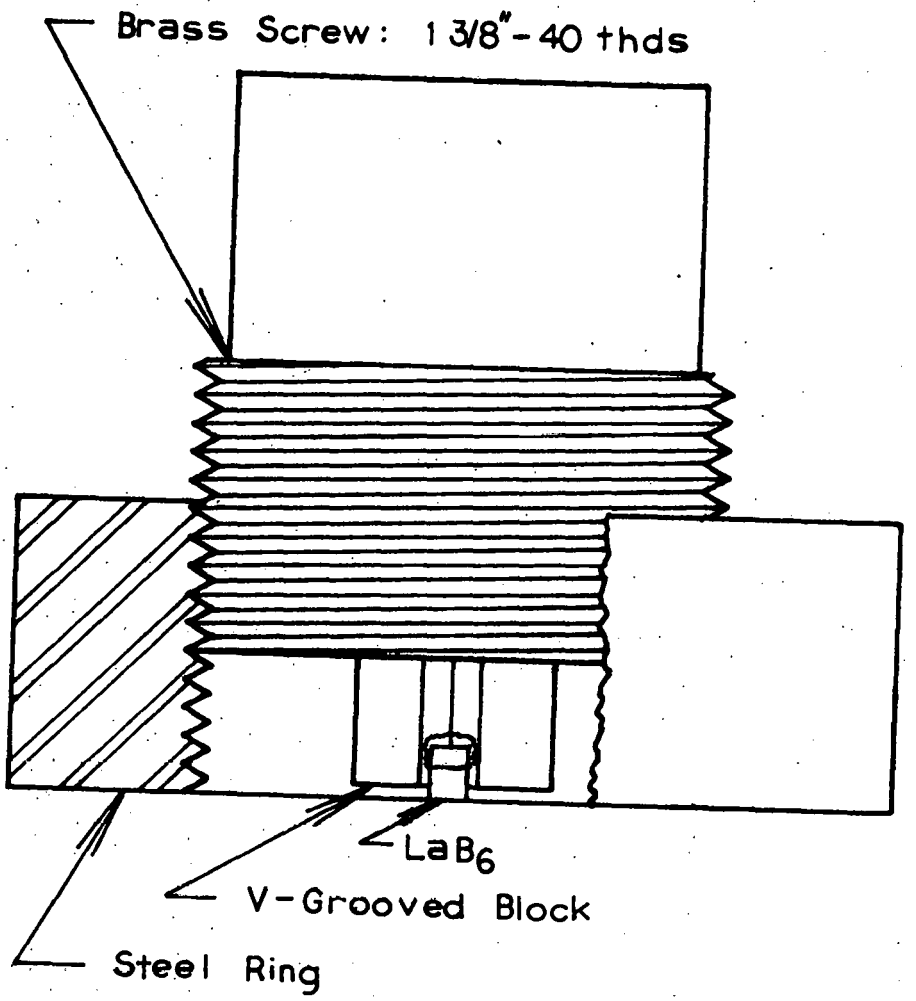

Figure 2. Gringing jig used to polish flat face on crystals

brass screw in the stainless steel ring, the sample could be advanced into the abrasive surface while maintaining axial alignment of the sample. In this manner, flat surfaces of desired planes could be obtained from axially oriented single crystals for the purpose of work function measurements.

The following orientations were prepared from 1 mm diameter type A crystals: (100), (110), and (111). These samples were hand lapped through 600 grit SiC paper using water as a lubricant. This provided a very flat surface, but not a scratch-free surface. Faces of 1½ mm diameter type C material were prepared similarly for (110) and (100) orientations. A further improvement in surface condition was obtained by polishing the 600 grit surface with Linde A, 0.2 μm Al_2O_3. The Linde A material was mixed with distilled water to form a slurry. This slurry was used with a vibrating wax lap to produce a very flat scratch-free surface. A 1 mm diameter crystal of type A material with a (346) orientation was polished in this manner for 24 hours on the vibratory wax lap. Approximately 70 hours were needed to produce similar surface quality for a 2½ mm diameter crystal of type A material. The long polishing times are due to the extreme hardness of LaB_6, 2770 kg/mm^2 (22). Thus, the surface removal rate was very slow. For a 2½ mm diameter crystal of the type C material, the use of Linde A was abandoned. Instead, the 600 grit surface was polished with a nylon vibratory lap using Hypereze 0.4 μm diamond compound. This resulted in a satisfactory surface finish

after approximately 12 hours polishing.

The single crystal rods used in this study are listed in Table 2. The rod diameter, number of zone refining passes, and the type of argon used are given for each. Where pertinent, the crystallographic orientation of the rod axis is included.

Chemical Analysis

The degree of purification achieved by the arc float zone refining was systematically studied by multiple analyses of the starting blank materials and the resulting zone refined rods. (Preliminary results of the purification have been published (23)). Several chemical analysis techniques were employed: mass spectroscopy, wet chemical analysis, vacuum fusion, and combustion analysis. The dimension of the 1 mm diameter rods was the ideal sample size for mass spectroscopic analysis. Two different spectroscopic techniques were used in this study. The first was used to analyze the distribution of metallic impurities along the zone refined rod and is similar to one described elsewhere (24). This technique permitted milliprobe type analysis of several points along the length of the zone refined rod using a 7 mil (0.18 mm) diameter, pure gold probe as a counter electrode. This provided spark excitation and analysis at localized spots with a spacial resolution of about 0.5 mm. This analysis was performed on a type B, single pass zone, refined rod. Two hot pressed blanks of the same material were used as the starting rods. Probe analyses were performed at regular intervals along the

Table 2. Single crystal rods

Crystal	Diameter (mm)	Number of zone passes	Argon	Orientation of axis
MA-7	1	1	Commercial	< 110
MA-8	1	1	Commercial	< 100 >
MA-11	1	1	Commercial	---
MA-14[a]	1	3	Commercial	< 346 >
MA-15[a]	1	3	Commercial	< 110 >
MA-19	1	1	Commercial	< 111 >
MA-20[a]	1	3	Commercial	< 100 >
MA-21[a]	1	3	Commercial	< 111 >
MA-23	1	1	Commercial	< 100 >
MA-36[a]	2½	2	Commercial	< 321 >
MA-37	1	1	Commercial	< 100 >
MB-2	1	1	Commercial	< 100 >
MB-4	1	1	Commercial	---
MB-8	1	6	Commercial	< 100 >
MC-1	2½	1	Commercial	---
MC-2	2½	1	Ultra zero	---
MC-3	2½	2	Ultra zero	< 321 >
MC-4[a]	2½	3	Ultra zero	< 321 >
MC-9	1	1	Ultra zero	< 110 >

[a]Crystals sent to Dr. L. Swanson for work function measurements.

Table 2. Continued

Crystal	Diameter (mm)	Number of zone passes	Argon	Orientation of axis
MC-10	1	1	Ultra zero	< 321
MC-11	1	2	Ultra zero	< 100 >
MC-12[a]	1½	3	Ultra zero	< 100 >
MC-13[a]	1½	3	Ultra zero	< 110 >
MD-1	2½	3	Ultra zero	---

resulting rod, starting at the hot pressed blank rod approximately 5 mm above the initial zone, and finishing at the final molten zone. This showed, among other facts, that the purity of the zone refined rod was uniform from the initial zone to nearly the final zone. Thus, results of analyses from the middle of the zone refined rod were just as reliable an indication of the concentration of contamination present as results from near the start of the refined rod. This observation provided the confidence needed for the use of a second mass spectroscopic technique.

In the second technique, self-arc mass spectroscopy, the two mating ends of a sectioned rod were sparked together as self electrodes. Sample length considerations for this method necessitated sectioning the zone refined rod at the center. From the results of the gold probe analysis, the analysis at this mid-point was considered representative of the refined material. The standard procedure for the zone melting of 1 mm diameter rods was used in preparation of analysis samples. Two hot pressed blanks of the same lot were used as starting rods for all zone refined rods analyzed by self-arc mass spectroscopy. Approximately one-half of the lower blank rod was solidified by the arc zone melting technique. The rod was then sectioned at the center of the remaining unsolidified portion and at the center of the solidified portion using EDM or a diamond saw. The samples were ultrasonically cleaned in acetone, freon, and methanol. The mating surfaces to be arced were heavily

electropolished in the perchloric solution to remove any surface contamination.

To provide a sufficient sample, approximately 100 mg for the other chemical analyses, rods larger than 1 mm in diameter were needed. Thus, 2½ mm diameter rods, approximately 30 mm in length, were solidified by the float zone technique. (Due to heat dissipation problems in the chamber, this was the maximum diameter that could be zone refined.) These rods were sectioned with a diamond saw according to the method illustrated by Figure 3. Each section was identified by its alphabetic letter. For example, after sectioning MC-1, the section containing the initial zone was coded as MC-1-A. Since each section was approximately 5 mm in length, the position of the analyzed sample relative to the initial zone can be estimated from the alphabetic suffix. The sections were ultrasonically cleaned and electropolished to remove any surface contamination. Analyses for lanthanum and boron were performed on some 1 mm diameter rods. Because of the lower sample weight, they provided a less precise determination of B/La ratio than obtained for the 2½ mm diameter samples. Gravimetric chemical analysis was used to determine the lanthanum and boron content and the technique is described in the Appendix. Vacuum fusion and combustion analyses were done for oxygen, nitrogen, hydrogen, and carbon. Thus, the concentrations of all the elements were analyzed.

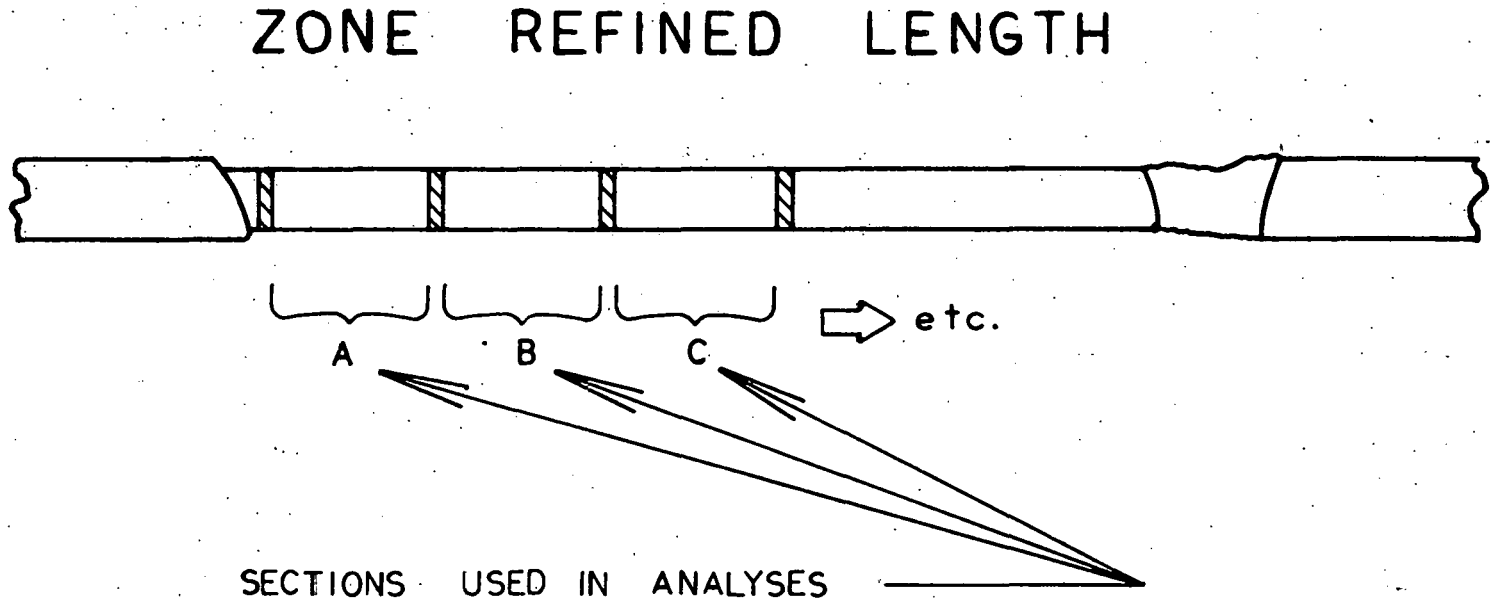

Figure 3. Sketch of rod sectioning

Temperature Measurements

The melting point of two 2½ mm diameter rods of lot C material was measured with a micro-optical pyrometer. The pyrometer was used to measure the temperature of the solid rod near the solidifying interface, opposite the dc arc. In this manner, interference from the radiation of the dc arc was avoided with the large diameter rods. Absorption corrections for the glass were determined by a standard technique using a National Bureau of Standards (NBS) tungsten ribbon lamp. The emissivity correction was calculated using

$$\frac{1}{T_{true}} - \frac{1}{T_{app}} = \frac{\lambda}{C^2} \ln \epsilon_\lambda \qquad (4)$$

where T_{true} = true absolute temperature of material

T_{app} = absolute temperature apparent to observer

λ = wavelength of radiation

ϵ_λ = emissivity of material

C^2 = constant, 14388 $\mu m\,^oK$

The value of the emissivity of solid LaB_6 at $\lambda = 0.65$ μm used in the calculations was 0.80 (8,25,26). The apparent temperature was determined to be the sum of the observed absorption and the pyrometer reading. The temperature scale of this pyrometer was compared with that of Leeds-Northrup pyrometer calibrated by NBS. Both scales agreed within the experimental precision of the comparison, $\pm$ 2°C.

Density Measurements

Densities of the rods were determined by a hydrostatic weighing technique (27,28,29). Three weighing measurements were made for each density determination: (i) the weight of the sample in air; (ii) weight of suspension apparatus in the liquid; and (iii) weight of sample and suspension apparatus in the liquid. The equations of balance for these measurements are:

$$M_s - V_s\rho_a = W_s^a \tag{5}$$

$$M_B - V_B\rho_L = W_B^\ell \tag{6}$$

$$M_s + M_B - V_B\rho_\ell - V_s\rho_\ell = W_A^\ell \tag{7}$$

where M_s = mass of sample

M_B = mass of suspension basket

V_s = volume of sample

V_B = volume of suspension basket

ρ_a = density of air

ρ_ℓ = density of liquid

W_B^ℓ = weight of basket in liquid

W_s^a = weight of sample in air

W_A^ℓ = weight of sample and suspension basket in liquid

The weighings were made in a constant temperature-humidity room, thus the density of air was assumed constant in all weighings. The two liquid suspension weighings were made in quick succession. Hence, the

density of the liquid was also assumed to be constant. Therefore,

$$W_A^{\ell} - W_B^{\ell} = M_s - V_s\rho_{\ell} = W_s^{\ell}$$

and

$$\rho_s = \frac{M_s}{V_s} = \frac{W_s^a\rho_{\ell}}{W_s^a - W_s^{\ell}} - \frac{W_s^{\ell}\rho_a}{W_s^a - W_s^{\ell}} \qquad (8)$$

where the second term is the correction due to air buoyancy.

A Perkin-Elmer electrobalance was used for all weighings. The range selected on the electrobalance for the weighings had a digital readout of 000.00 mg and a setting reproducibility of 0.005 mg. The suspension apparatus consisted of an 80-mesh stainless steel basket suspended from a wire hook by an electropolished 15 μm diameter Chromel-P wire[1]. This arrangement resulted in the most reproducible liquid suspension weighings. The liquid used was distilled water. The temperature of the water was measured with a liquid mercury in glass thermometer. The density of the distilled water used in the calculations was taken from Tilton and Taylor's tabulated values of mg/ml versus temperature (30). The value 0.999973 was used to convert to gm/cm^3 (31).

Prior to weighings, the samples were cleaned by electropolishing in the perchloric acid methanol solution. After the samples were weighed in air, they were immersed in the beaker of distilled water.

---

[1]The original diameter of wire was 25 μm before electropolishing.

The beaker was placed in a vacuum desiccator. A vacuum was obtained with a mechanical pump to ensure that no air bubbles were trapped on the surface of the samples. One hour of time was allowed for obtaining thermal equilibrium. Then a series of weights alternating between that of the empty basket and that of the basket with a sample were made. The series of measurements took about one hour during which the temperature of the water did not change by more than $0.1^{o}C$. Due to the small amount of time the crystals spent in the water, any change in their volume resulting from a reaction with the water was considered negligible[1].

Lattice Parameter Measurements

X-ray analysis of LaB_6 material was done with a 114.6 mm Debye-Scherrer camera using filtered CuKa radiation. Two types of samples were used: powder and single crystal rod. The single crystal rod had a <100> axial orientation. By rotation about this axis, a sufficient number of spots were obtained in the back-reflection region. The region bathed in the beam had been electropolished to reduce the diameter from 1 mm to < 0.1 mm. Tungsten powder was used as an internal standard.

The powder samples were prepared by crushing a section of refined rod in a diamond mortar. These crushed pieces were then ground into

---

[1]However, if left in the water over a weekend, a nonconductive film would form over the areas of the samples.

a fine powder using an agate mortar and pestle. This powder was screened through 325 mesh.

The Debye-Scherrer films were read using a Kirem coincidence rule with 0.01 mm division dial indicator. Film shrinkage corrections were applied. No lines were observed which could not be attributed to LaB_6. Lattice parameters reported were calculated from a linear regression of a Nelson-Riley extrapolation of the data. The data were not corrected for index of refraction.

Evaluation of LaB_6 Cathodes

The 1 mm diameter, single crystal LaB_6 rods were evaluated as cathodes in a Cambridge S-4 SEM. An electron gun design, similar to that published in the literature (32), was used. A hot 5-turn 0.25 mm diameter tungsten coil provided radiative and electron bombardment heating. The coil had an inner diameter of 2.05 mm. Radiative shielding was provided by a tantalum canister. A 1.6 mm diameter hole was drilled in the canister to allow for the protrusion of the cathode tip.

The temperature of the cathode tip was measured in situ. A micro-optical pyrometer with a disappearing filament was used to measure the tip of the cathode. This pyrometer was fitted with an objective lens with approximately 18 inches focal length. This provided an enlarged image of the cathode. By lowering the anode, the pyrometer could be focused on the cathode tip through a hole drilled

into the gun chamber[1]. The hole was covered with a fused silica window. A removable cover was used to protect the window surface from condensation of any vapor present in the gun chamber.

The direct observation of the cathode tip allowed the temperature of the emitting surface to be known to the same precision as that of the pyrometer, $\pm$ 2°C. The absorption of the window was measured to be 15°C in temperature region of these experiments. The apparent temperature was then the pyrometer reading plus 15°C. Equation 4 was used to calculate the true temperature using this apparent temperature.

LaB_6 evaporation

Mass loss rates were evaluated by measurement of change in cathode tip diameter. Shadow graphs were taken of the cathode before assembly of the electron gun. Shadow graphs were again taken of the same view of the cathode after operation in the electron gun. The measured change in diameter was converted to mass loss rate based on the density of the cathode, 4.70 gm/cm^3, and the measured time the cathode was at temperature.

$$\Gamma = \frac{\Delta d}{2} \rho / t \qquad (9)$$

where Γ = mass loss rate

Δd = change in cathode diameter

---

[1]The gun chamber was furnished by Cambridge Instruments Limited.

ρ = density of cathode

t = time

Brightness measurements

The determination of brightness is a difficult measurement because it requires an accurate measurement of beam diameter, beam current, and beam divergence. (See Equation 1.) The determination is further complicated if a demagnified image of the electron source is used. The brightness of this image will be conserved only if two conditions are met: (a) the beam limiting aperture is completely filled, and (b) the image formed is aberration free. Both conditions must be obtained in order to measure the maximum brightness of the electron gun.

To ensure that the first condition was met, the electron gun was aligned with the electron optical axis of the SEM. Broers (33) recommends great care be taken in the alignment of the electron gun. He states that, due to the small crossover formed by the LaB_6 electron gun, the maximum brightness is not observed unless the electron gun is properly aligned. The alignment of the electron gun with the electron optical axis was done in the following manner. First, the final lens aperture, the beam limiting aperture, was centered on the optical axis. This condition was established by movement of two mechanical centering screws until an image observed at high magnification did not shift laterally as the focus of the final lens was changed. Next, centering of the electron beam within the aperture was

achieved by means of two shift coils contained in the scan coil assembly of the final lens. The beam was placed in a Faraday cage. The current, hereafter referred to as the cage current, was monitored with a specimen current amplifier. As the current in the shift coils was varied, the cage current was found to peak for a certain range of potentiometer settings. The beam was considered centered within the aperture when the cage current was peaked. Thirdly, the electron gun was mechanically centered over the anode. The electron gun was considered centered at the position which produced the maximum cage current. Finally, steps one through three were repeated until the cage current measured did not increase in value. The electron gun was then considered aligned with the electron optical axis.

Because aberration-free magnetic lenses do not exist, the second condition for constant brightness, an aberration-free image, cannot in a strict definition be obtained. The relationship between the image formed by a lens and the image formed by an aberration-free lens is given by

$$d_T^2 = d_o^2 + d_A^2 + d_D^2 + d_S^2 + d_C^2 \qquad (10)$$

where d_T = diameter of image formed by the magnetic lens

d_o = diameter of image formed by aberration-free lens

d_A = diameter increase due to lens' astigmatism

d_D = diameter increase due to diffraction

d_S = diameter increase due to spherical aberration

d_C = diameter increase due to chromatic aberration

The lens' astigmatism could be corrected by the use of an astigmator in the pole piece of the lens. This correction was verified by the measurement of the beam diameter in two mutually perpendicular directions. Diameters measured in both directions were equal, within experimental error, when the astigmator was properly adjusted. For a given lens and final lens aperture, the other aberrations of the image, formed at a given distance from the lens, are fixed and cannot be corrected. However, the total demagnification by the SEM lens system can be reduced until the difference between d_T and d_o is insignificant. This condition was confirmed by measurements which displayed a linear relationship between the beam current and beam diameter squared for the demagnification employed when measuring brightness.

The technique used to measure the beam diameter, beam divergence, and beam current was similar to that described by Verhoeven and Gibson (11). However, the technique was improved by the substitution of two devices used in these measurements. First, an X-Y plotter was used instead of an oscilloscope to measure beam profiles. This provided a permanent record and allowed the beam diameter to be determined with better precision. A new Faraday cage was constructed as shown in Figure 4. This cage had a 1000 mesh grid over the entrance hole. This provided mutually perpendicular edges and allowed the beam diameter to be measured in two orthogonal directions. (As previously mentioned, this provided confirmation of the proper setting of the astigmator.)

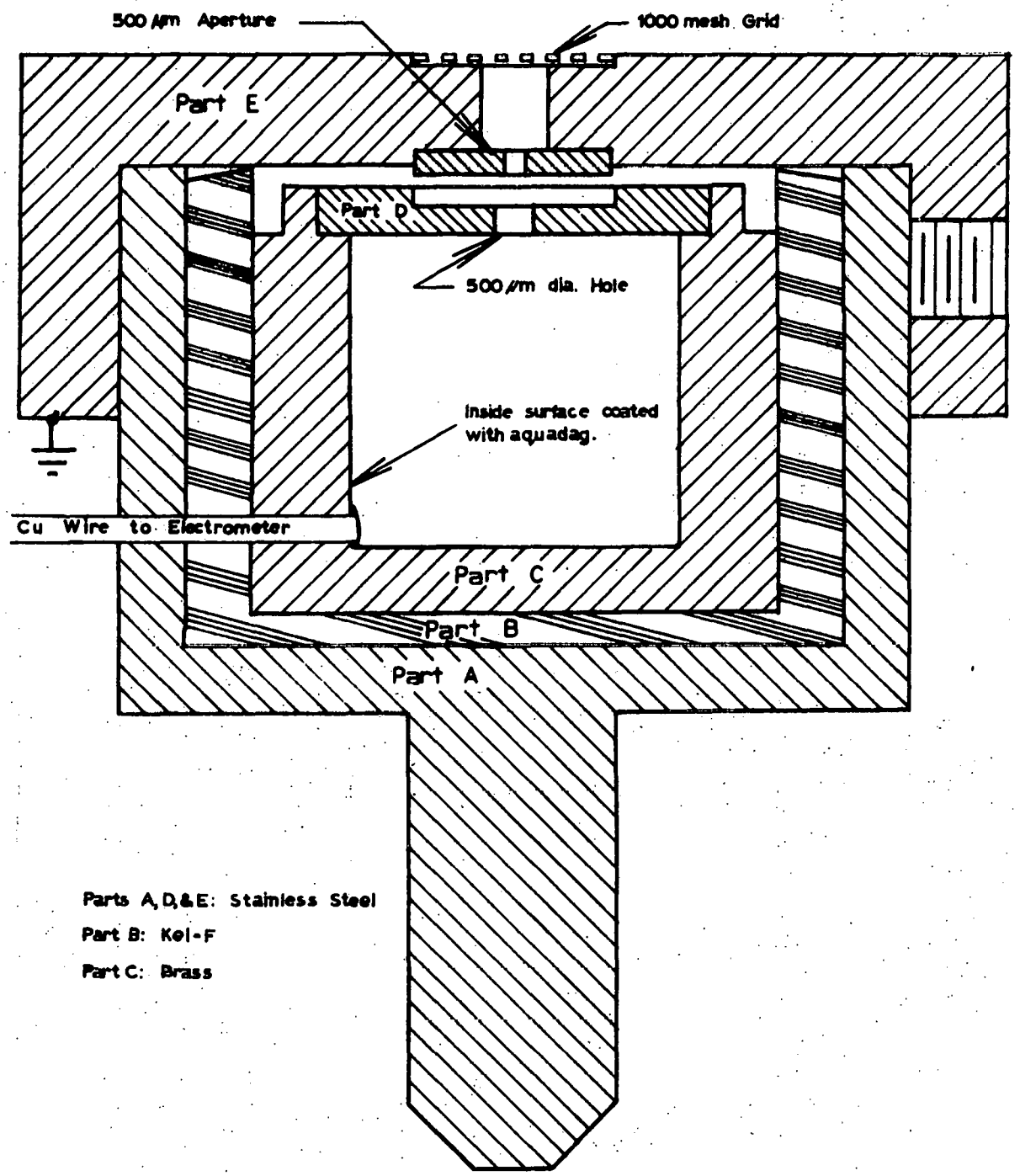

Figure 4. Sectioned view of Faraday cage

RESULTS

Crystallography

The arc float zone melting technique always produced single crystal rods. Even when a polycrystalline hot pressed rod was used as the starting rod, a single crystal resulted after two or three zone lengths of growth. The orientation of crystals grown in this manner were observed to be random. In the seeding experiments, the crystals which were grown had the orientation of their rod axis within $\pm 1^{o}$ of the desired orientation. Back-reflection Laue photographs taken along the rod axis and selected area channelling patterns of traverse sections were used to verify the above results. The sensitivity of the selected area channelling technique was such that an area as small as 2 μm in diameter misoriented by more than 0.5^{o} could have been detected.

Metallography

The metallographic examination of the LaB_6 material was done with a Unitron Series N metallograph and a Cambridge S-4 SEM. The SEM was equipped with an energy dispersive spectrometer (EDS). This allowed analysis for all elements heavier than sodium. Analysis of single crystal sections in the SEM with EDS revealed no regions which contained any elements other than lanthanum. However, examination in the SEM, of the hot pressed rods of A and C material, showed regions of second phase material to contain tungsten. These regions appeared

gold colored when observed with the metallograph. Metallographic preparation of single crystal material from lot A resulted in a uniform flat surface. For these crystals, no surface defects or second phase was observed with the optical microscope after polishing through Linde A on the wax lap. However, when sections of single crystal material from lot C, having a 2½ mm diameter, were polished, a pitted surface resulted. These pits were from 0.5 μm to 2 μm in diameter. Examination of these pits in the SEM revealed a substructure contained in some pits. The analysis of this structure with EDS revealed energy peaks due only to lanthanum. Because of the small size, quantitative analysis could not be obtained for the lanthanum concentration.

Chemical Analysis

Mass spectrometry

The results of the mass spectrometry were semiquantitative since standard samples were not available. The absolute error in the determined levels was estimated to be ± 100%. However, on the basis of replicated analyses and previous experience, the relative differences in concentration between samples were significant at the ± 30% level. The results of the mass spectrometric analysis, using the gold probe, revealed interesting phenomena about the purification of LaB_6. One was the uniformity of the contamination level along the zone refined length. Figure 5 illustrates this uniformity for three representative elements: tantalum, iron, and chromium. The relative differences in

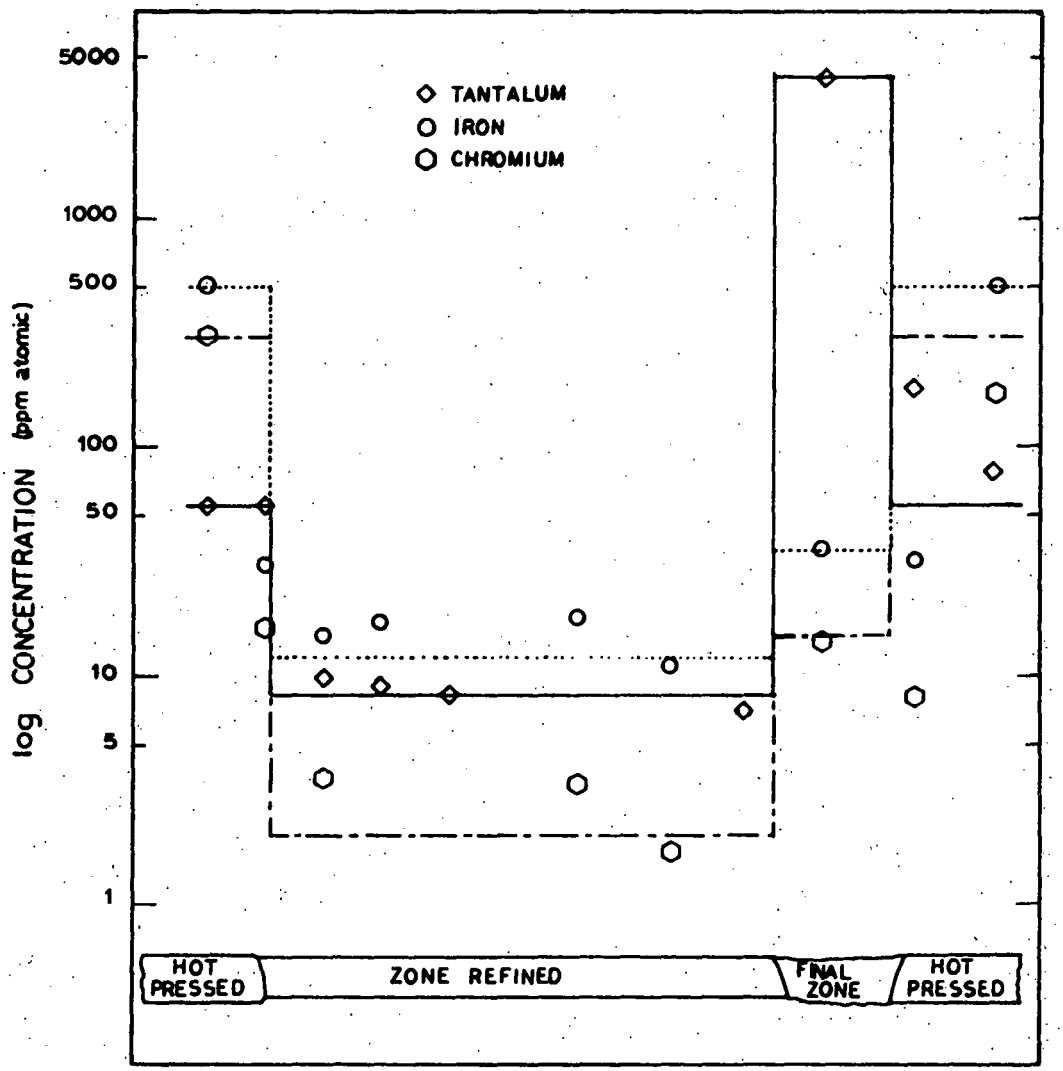

Figure 5. Impurity concentration profile of zone refined rod

concentration between areas analyzed in the zone refined rod were not considered significant. Another phenomenon revealed by the gold probe analysis, was that certain elements present in the starting hot pressed blank were found greatly reduced in concentration in both the purified section and the final solidified zone. Thus, purification was not achieved simply by rejection of the impurity into the liquid, the classical mode of purification, rather, purification of these elements was enhanced by vaporization from the molten zone. This is shown in Table 3 for the elements marked with an asterisk. The higher melting elements were found at a high concentration in the final solidified zone and were not vaporized. The rare earth elements also appeared not to be vaporized.

The results of the self-arc mass spectrometric analyses of three different lots of LaB_6 material are given in Table 4. There was considerable difference in the impurity content of the lot A material. The total impurity content, approximately 0.7 $^{w}/o$, of the starting blank is much higher than would be expected based upon the quoted purity, 99.9 $^{w}/o$. However, the zone refining effect was extremely effective at purifying even this lot. After three zone passages, the total impurity content of both lot A and lot C crystals was reduced to approximately the same level even though the starting impurity content was significantly larger for lot A.

Another result noted, was the removal of tantalum. With the dc arc technique, the tantalum electrode would transfer tantalum to the

Table 3. Mass spectrometric analysis of LaB_6 using gold probe (atomic ppm)

Element	Starting blank	Zone refined	Final zone
Ta	55	8	4000
W	160	< 2	2900
Mo	38	< 5	360
Y	8	< 3	65
*Al	10	< 0.5	< 0.5
*Ca	130	< 5	< 5
*Co	10	< 1	< 1
*Cr	300	2	15
*Cu	20	< 1	< 1
*Fe	500	12	35
*Mn	7	1	1
*Ni	200	10	40
*Sr	6	< 0.5	< 0.5
*Ti	27	3	15

Table 4. Spark source mass spectrometric analysis of LaB_6 (atomic ppm)

Element	Lot B		Lot A			Lot C		
	Starting blank	1-Pass crystal	Starting blank	1-Pass crystal	3-Pass crystal	Starting blank	1-Pass crystal	3-Pass crystal
Al	40	2	2400	0.09	0.07	3000	< 0.08	< 0.08
Ba	17	< 1	15	< 2	< 0.9	14	< 1	< 2
Ca	2200	< 5	1200	< 1	< 0.03	50	< 1	< 0.2
Ce	14	11	< 0.5	< 0.4	< 0.3	5	2	4
Co	20	< 0.3	1800	40	< 0.08	10	< 0.9	< 0.3
Cr	400	< 0.2	500	7	< 0.08	150	2	0.7
Cu	160	< 0.3	17	< 0.3	0.3	62	< 0.1	< 0.1
Fe	850	15	4200	120	30	1600	20	< 0.7
Hf	15	< 3.4	10	< 3	< 3	4	3	3
K	70	< 0.06	36	0.3	< 1.5	2	< 0.03	< 0.04
Mg	10	< 3	13	< 1.5	< 0.3	50	< 0.08	< 0.1
Mn	13	< 0.1	45	< 0.1	< 0.08	90	< 0.07	< 0.01
Mo	30	< 1.4	2000	370	< 1.5	600	15	2.4
Na	130	< 0.7	30	< 1	0.5	100	< 0.2	< 0.4
Nd	5	< 1.5	12	13	5	6	8	10

Table 4. Continued

Element	Lot B		Lot A			Lot C		
	Starting blank	1-Pass crystal	Starting blank	1-Pass crystal	3-Pass crystal	Starting blank	1-Pass crystal	3-Pass crystal
Ni	110	< 0.5	2400	70	< 1	600	20	0.8
Pr	8	3	18	13	5	3	3	5
S	230	0.5	290	0.7	< 0.04	100	< 0.1	< 0.1
Si	190	< 0.35	270	7.1	< 1	100	< 4	< 1
Sr	7.1	< 0.04	48	0.1	< 0.01	50	< 0.1	< 0.03
Ta	85	3	50	10	< 0.7	7	< 0.3	< 0.5
Ti	30	< 0.4	900	200	0.5	200	< 0.08	< 0.4
V	5	< 0.03	70	10	< 0.02	10	0.5	0.1
W	140	20	3000	500	< 2	500	20	8
Y	10	2	10	3	0.9	3	0.6	0.7
Zr	70	11	470	160	< 0.8	200	4.2	5
Total atomic	4860	< 80	19800	1500	< 60	7500	100	< 70
Total weight	0.13 w/o	< 0.005 w/o	0.7 w/o	0.085 w/o	< 0.0023 w/o	0.2 w/o	0.005 w/o	< 0.003 w/o

molten zone. Evidently the distribution coefficient of tantalum in LaB_6 was sufficiently low that the tantalum concentration was reduced in the zone refined rod.

Carbon analysis

The carbon concentration could not be measured by mass spectrometric analysis due to interference of boron. The data in Table 5 were obtained by combustion analysis. There was a large variability of the carbon concentration in the hot pressed starting blanks and the carbon content was significant. Comparison of the carbon content found in the LaB_6 powder indicates a significant contamination of the hot pressed material. This could result from the use of graphite dies in the hot press process. The residue left after the acid dissolution of the hot pressed samples implied graphite was present. The surface preparation of the blank rod served to reduce the carbon concentration significantly. This was revealed by comparing the analyses of the as-spark-cut and the electropolished starting blanks of lot C. Successive passages of the molten zone caused a reduction in the carbon concentration as revealed by comparing analyses of MC-2-B and MC-4-D. The reason that the carbon content of MC-1-B is higher than MC-2-B is unknown. The higher carbon content of MC-1-B may have resulted from inadequate surface cleaning during preparation of the starting blanks of this sample or from the use of a lower purity argon gas as shown in Table 2.

Table 5. Carbon analysis of LaB_6

Sample	Number zone passes	w/o C	C/La atom ratio
#1155 LaB_6 powder	AR[a]	0.063 0.064	0.0107 0.0109
Lot C as-spark-cut	AR	0.296 0.346	0.0499 0.0583
Lot C electropolished	AR	0.189 0.185	0.0319 0.0312
Lot D electropolished	AR	0.145 0.137	0.0249 0.0235
MA-36-A	2	0.070	0.0120
MC-1-B	1	0.175	0.0292
MC-2-B	1	0.0715	0.0120
MC-4-D	3	0.0055	0.00092
MD-1-B	3	0.007	0.0010

[a]As received material.

Vacuum fusion

Vacuum fusion analyses were done only for lot C material. Comparison of mass spectrometric analyses of the lot C material showed good agreement with the oxygen results of the vacuum fusion analyses. The mass spectrometric estimates of the oxygen concentration for lot A material were included in Table 6. Both techniques showed a large reduction in the oxygen concentration after a single passage of the molten zone. Additional passages did not reduce the oxygen content. The concentration of nitrogen and hydrogen found by vacuum fusion analysis was reduced below the detection limit after three passages.

Boron and lanthanum composition

The dissolution in the nitric acid of the hot pressed samples of LaB_6 left a minute black residue in the Teflon cup. However, the dissolution of the zone refined samples was complete with no residue. It was concluded that the residue was free carbon. This was the only element, which was insoluable in hot nitric acid, and of sufficient concentration to be noticeable.

The results from the chemical analysis of the 100 mg portions of LaB_6 powder #1155 given in Table 7 gave a standard deviation of the B/La atom ratio equal to 0.03. Table 8 gives the chemical analyses for hot pressed and zone refined materials. All of these samples weighed approximately 100 mg except the first four which weighed between 10 and 30 mg. Hence, the error in the B/La ratio is expected to be larger than 0.03 for the first four samples. The B/La

Table 6. Vacuum fusion analysis of LaB_6

Sample	Oxygen ppm weight	Oxygen ppm atomic	Nitrogen ppm weight	Nitrogen ppm atomic	Hydrogen ppm weight
Lot C	370	4600	13	190	27
MC-1-C	16	200	8	100	ND[a]
MC-2-C	15	200	5	70	ND
MC-4-C	20	250	ND	ND	ND
Lot A	--	4000[b]	--	--	--
MA-11	--	330[b]	--	--	--

[a]None Detected.

[b]Mass spectrometric estimate.

Table 7. Chemical analysis of #1155 LaB_6 powder

LaB_6	w/o La	w/o B	B/La atom ratio
Solution 1	67.94	31.83	6.02
	68.22	31.77	5.98
Solution 2	68.09	31.57	5.96
	68.09	31.64	5.97
Theoretical	68.17	31.83	6.00

Table 8. Chemical analysis for lanthanum and boron

Number zone passes	Sample	Weight percent La	Weight percent B	Mass balance	B/La atom ratio
1	MA-11	66.18	29.33	96.51	5.61
	MA-11	68.37	32.54	100.91	6.12
1	MB-4	67.12	31.00	98.12	5.93
	MB-4	67.51	31.19	98.70	5.94
AR[a]	Lot A Start blank	66.40	30.94	97.34	5.99
1	MA-23 plus MA-19	68.2	30.7 31.1 31.5	99.3	5.86
2	MA-36-B	68.2	31.1 31.2	99.3	5.86
AR	Lot B Start blank	67.1	31.7	98.9	6.07
AR	Lot C Start blank	68.60	31.03	99.63	5.81
1	MC-1-A	69.93	30.97	100.90	5.69
	MC-1-D	69.22	30.80	100.02	5.71
	MC-1-F	69.04	30.64	99.68	5.70
	MC-1 Final zone	68.08	27.21	95.29	5.13
1	MC-2-E	68.81	30.74	99.55	5.74
3	MC-4-A	69.58	31.04	100.62	5.73
	MC-4-F	69.20	31.02	100.22	5.76

[a]As received material.

Table 8. Continued

Number zone passes	Sample	Weight percent La	Weight percent B	Mass balance	B/La atom ratio
	Lot D	67.15	30.28		
AR	Start blank	67.37	30.02	97.4	5.75[b]
			30.02		
3	MD-1-D	68.45	31.20	99.7	5.86
		68.45	31.33		

[b]This value may be in error because a large amount of residue was observed after dissolution of sample.

ratios of the zone refined rods were significantly different from the stoichiometric 6.00. The B/La ratio remained constant over the length of the zone refined rod, MC-1. The final solidified zone had a higher concentration of lanthanum to boron than the zone refined rod. It was also noted that single crystals from lot A material had a significantly higher B/La ratio than those prepared from lot C material.

Melting Point

The melting point of two rods from lot C was measured with an optical pyrometer. The melting point of crystal MC-1 was 2473°C[1] and that of crystal MC-4 was 2457°C. In a similar manner the melting point of high purity niobium rods was also measured. The average of six determinations, using an emissivity of 0.40 (34) was 2465°C. The accepted value for the melting point of niobium is 2468°C (35).

Density and Lattice Parameter

Since the chemical analyses indicated the crystals to be off stoichiometry, precision density and lattice parameter measurements were performed. The results of the density measurements are listed in Tables 9 and 10. The error of the density technique was checked by the measurement of standards of known density. Based on these results, the probable error in the measured density of the crystals was established to be ± 0.005 gm/cm^3. Hence, the density of the lot C

---

[1] All temperatures quoted in this thesis include correction for absorption and emissivity as described previously.

Table 9. Density of standards

Sample	Measured densities (gm/cm^3)	Standard density
Al	2.695, 2.696, 2.698	2.6980
Ge-I	5.326, 5.330, 5.334 5.326	5.3267
Ge-II	5.331, 5.320, 5.322 5.320, 5.322	5.3267

Table 10. Density of LaB_6 crystals

LaB_6 crystal	Measured density (gm/cm^3)
MA-7	4.70
MB-2	4.71
MB-8	4.71
MC-1-E	4.708
MC-3-A	4.716
MC-4-E	4.701 4.707
MD-1-B	4.698
MD-1-C	4.703

crystals would be between 4.70 and 4.71 gm/cm^3 with a 90% confidence interval. Measurements of crystals from lots A and B were done with smaller samples. Consequently, the error for those crystals was greater.

The precision lattice parameters were obtained at approximately 22^oC. Measurements were based on $\lambda CuK\alpha_1 = 1.540562\text{Å}$ (36). The results of the measurements are given in Table 11. The value in parenthesis was the standard deviation of the last digit for the intercept of the Nelson-Riley extrapolation.

Cathode Evaluation

The lifetime measurements were made at two temperatures, 1975^oK and 1905^oK. After 196 hours at 1975^oK, a reduction of 0.16 mm was measured in the diameter of a cathode at the tip. This gave a calculated flux loss of 5.34×10^{-8} $gm/cm^2 \cdot sec$. After 280 hours at 1905^oK, the measured reduction in diameter was 0.09 mm. This measurement was impaired by several excursions up to 2000^oK for "firing" of the cathode. The calculations gave a flux loss of 2×10^{-8} $gm/cm^2 \cdot sec$. This would be equivalent to approximately a 2,500 hour lifetime for a 1 mm diameter cathode evaporated 75% of its radius.

The brightness was measured at various temperatures. Figure 6, illustrates the increase in brightness found with temperature. From the figure, it was concluded that the electron gun was not significantly space charge limited at the temperatures where brightness measurements were taken. These measurements also revealed that the

Table 11. Precision lattice parameters

Sample	a_o	w/o C	B/La atom ratio
#1155 LaB_6	4.1567(2)	0.063[a]	5.98
MA-37	4.1567(1)	--	(5.86)[b]
MC-4-E	4.1564(1)	0.006	5.75
MC-1-E	4.1558(2)	0.175	5.70

[a] It is believed the majority of this carbon is free carbon because of black residue left after dissolving in acid. (See text.)

[b] Estimated from data on MA-23 (see Table 8).

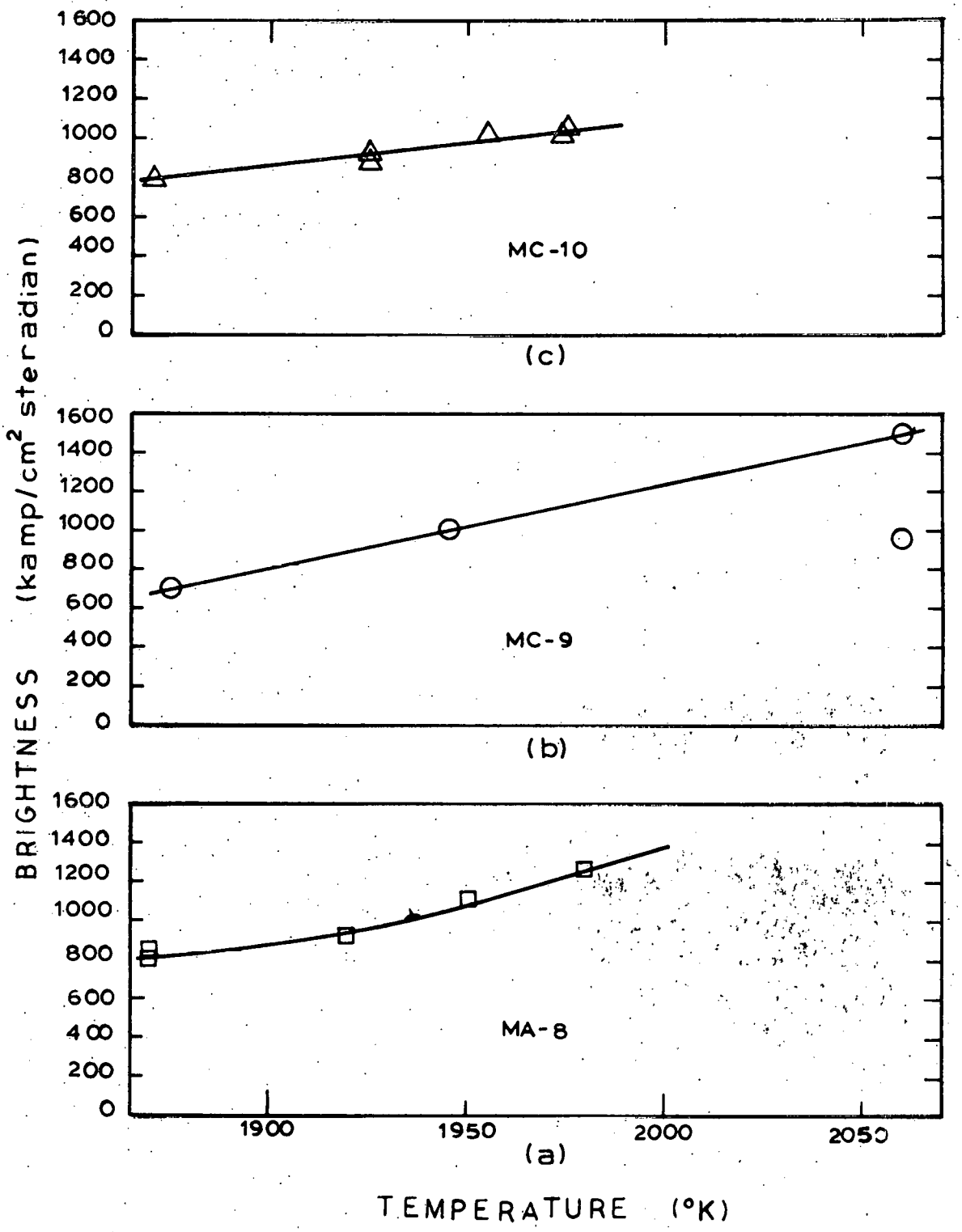

Figure 6. Brightness vs temperature plots for cathodes

probe diameter consistantly decreased with a rise in the cathode temperature as listed in Tables 12, 13, and 14. It was found that the optimum conditions of the electron gun were not always the same for every cathode. Once the conditions were established, consistent brightness values were measured. (See Tables 12, 13, 14, and 15.) At a cathode temperature between 1870 and 1880°K, the average measured brightnesses[1] of lot C crystals of (001), (321), and (110) orientations were 9.8×10^5, 8.1×10^5, and 6.8×10^5 amp/cm^2·steradian, respectively. The brightness of a single crystal from lot A with (001) orientation was measured to be 8.0×10^5 amp/cm^2·steradian. The relative error of these measurements based on the precision of the diameter and current measurements was 8%. These data showed that for the lot C material the (001) orientation was significantly brighter than the (110) orientation at 1875°K.

Thermionic Properties

The method of work function measurement utilized the crystal as a thermionic source and application of Equation 3. The "effective" work function ϕ_e was measured at each temperature according to

$$\phi_e = \kappa T \ln(J/120T^2) \qquad (11)$$

where $\bar{r}$ in Equation 3 is assumed to be zero and A is 120 amp °K^2/cm^2. The effective work function values ϕ_e are given in Figure 7 as a

---

[1] All brightness measurements were done at an accelerating voltage of 20 kV.

Table 12. Brightness measurements for MA-8, (001)

Pyrometer reading (°C)	Corrected temperature (°K)	Anode-bias settings	Beam current meter (μ amp)	Pressure (μ Torr)	Probe radius o (A)	Probe current (n amp)	Cathode brightness (k amp/cm^2 steradian)
1555	1875	6-3	238	1.0	1860	108	460
1555	1875	6-2	181	1.0	1390	81	620
1555	1875	6-1	140	1.0	990	52	780
1555	1875	5-2	250	1.0	1940	113	440
1555	1875	5-1	204	1.0	1390	83	630
1555	1875	5-1	204	1.0	1360	83	660
1555	1875	5 3/4-1	154	1.0	1040	57	780[a]
1550	1870	5 3/4-1	156	0.5	1150	71	790[a]
1550	1870	5 3/4-1	156	0.5	1110	65	780[a]
1550	1870	5 3/4-1	156	0.5	1040	63	850[a]
1600	1920	5 3/4-1	160	0.5	930	55	930
1630	1950	5 3/4-1	162	0.5	850	55	1130
1650	1970	5 3/4-1	164	0.5	820	58	1270

[a]Average of these four measurements is 8.0 x 10^5 amp/cm^2 steradian.

Table 13. Brightness measurements for MC-9, (110)

Pyrometer reading (°C)	Corrected temperature (°K)	Anode-bias settings	Beam current meter (μ amp)	Pressure (μ Torr)	Probe radius (A)	Probe current (n amp)	Cathode brightness (k amp/cm^2 steradian)
1550	1870	6-2	155	0.50	845	32	660
1550	1870	6-2	155	0.50	860	32	630
1555	1875	6-2	155	0.35	900	37	670
1555	1875	6-2	155	0.35	950	37	600
1550	1870	6-3	205	0.50	1190	43	450
1550	1870	6-3	205	0.50	1155	43	470
1555	1875	6-3	206	0.35	1250	45	420
1555	1875	6-3	206	0.35	1300	45	390
1555	1875	5 1/2-2	186	0.30	915	40	700[a]
1555	1875	5 1/2-2	186	0.30	880	38	720[a]
1555	1875	5 1/2-2	185	0.35	1030	45	620[a]
1555	1875	5 1/2-2	186	0.20	950	42	680[a]

[a]Average of these four measurements is 6.8 x 10^5 amp/cm^2 steradian.

Table 13. Continued

Pyrometer reading (°C)	Corrected temperature (°K)	Anode-bias settings	Beam current meter (μ amp)	Pressure (μ Torr)	Probe radius (Å)	Probe current (n amp)	Cathode brightness (k amp/cm^2 - steradian)
1625	1945	5 1/2-2	195	0.30	990	67	1000
1735	2060	5 1/2-2	205	0.40	810	68	1500
1735	2060	5 1/2-2	205	0.40	1025	68	950

Table 14. Brightness measurements for MC-10, (321)

Pyrometer reading (^{o}C)	Corrected temperature (^{o}K)	Anode-bias settings	Beam current meter (μ amp)	Pressure (μ Torr)	Probe radius o (A)	Probe current (n amp)	Cathode brightness (k amp/cm^2 steradian)
1555	1875	8-4	177	0.3	1080	52	660
1555	1875	8-3	121	0.3	950	33	560
1555	1875	8-2	83	0.3	840	18	380
1555	1875	7-4	235	0.3	1170	59	630
1555	1875	7-3	180	0.3	1015	43	610
1555	1875	7-2	126	0.3	830	29	620
1555	1875	7-1	92	0.3	810	18	400
1562	1882	6-3	235	0.3	940	50	830[a]
1562	1882	6-3	235	0.3	930	50	850[a]
1562	1882	6-3	235	0.3	990	50	750[a]
1562	1882	6-2	182	0.3	865	39	760
1562	1882	6-1	141	0.3	800	28	640

[a]Average of these five measurements is 8.1×10^5 amp/cm^2 steradian.

Table 14. Continued

Pyrometer reading (^{o}C)	Corrected temperature (^{o}K)	Anode-bias settings	Beam current meter (μ amp)	Pressure (μ Torr)	Probe radius o (A)	Probe current (n amp)	Cathode brightness (k amp/cm^2 steradian)
1562	1882	5 1/2-2	215	0.3	820	39	850[a]
1562	1882	5 1/2-1	181	0.3	820	32	700
1562	1882	5-1	204	0.3	830	33	710
1562	1882	5-1	204	0.3	840	33	690
1555	1875	5 7/8-3	240	0.3	990	52	780[a]
1605	1925	5 7/8-3	246	0.3	990	62	930
1635	1955	5 7/8-3	250	0.3	955	63	1020
1655	1975	5 7/8-3	255	0.3	945	63	1040
1653	1973	5 1/2-2	224	0.3	870	52	1010
1605	1925	5 1/2-2	218	0.3	900	49	890

Table 15. Brightness measurements for MC-11, (001)

Pyrometer reading (^{o}C)	Corrected temperature (^{o}K)	Anode-bias settings	Beam current meter (μ amp)	Pressure (μ Torr)	Probe radius (A)	Probe current (n amp)	Cathode brightness (k amp/cm^2 steradian)
1562	1882	6-3	220	4.0	1690	102	530
1557	1877	6-3	218	1.0	1350	113	910
1557	1877	6-3	218	1.0	1450	113	790
1550	1870	6 3/4-3	155	0.6	1700	97	500
1557	1877	5-2	230	0.9	1600	118	680
1550	1870	5 1/4-1	166	0.6	1760	88	420
1550	1870	5 1/2-1	150	0.6	1320	80	680
1560	1880	6-3	208	1.5	1280	110	990[a]
1560	1880	6-3	210	0.9	1250	100	940[a]
1560	1880	6-3	205	0.9	1170	96	1030[a]
1560	1880	6-3	205	0.9	1170	96	1030[a]
1560	1880	6-3	205	0.9	1250	96	900[a]
1560	1880	5 3/4-3	218	0.6	1230	113	1100

[a]Average of these five measurements is 9.8×10^5 amp/cm^2 steradian.

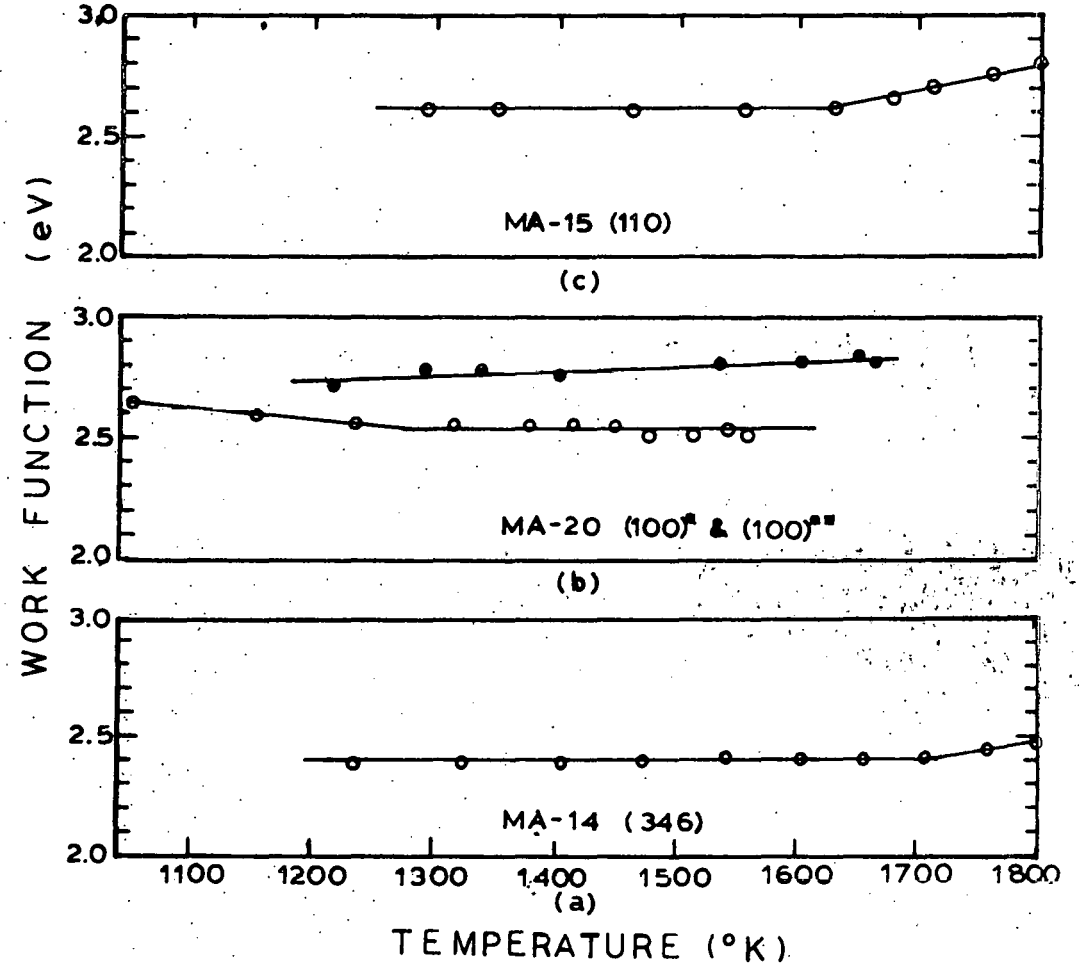

Figure 7. **Zero field thermionic work function vs temperature plots for LaB_6 single crystals** (Measurements by L. Swanson, Oregon Graduate Center, Beaverton, Oregon)

function of temperature. The data of the upper curve 100* of Figure 7b are measurements made on MC-20 after an initial thermal cleaning; the data of lower curve 100** are measurements made on MC-20 after a prolonged heating at 1800°K.

A second method of work function measurement, the FERP method described in detail elsewhere (37), was also used to measure the change in work function caused by the removal of surface oxygen. The crystal MA-15 was exposed at room temperature to oxygen. After heating the crystal for 60 seconds at a given temperature, the work function and Auger electron spectroscopy (AES) signal were measured. Figure 8 shows the work function and AES signal strengths as a function of 60 second heating at the indicated temperature. The minimum work function of 2.60 eV at 1600°K was reproducible.

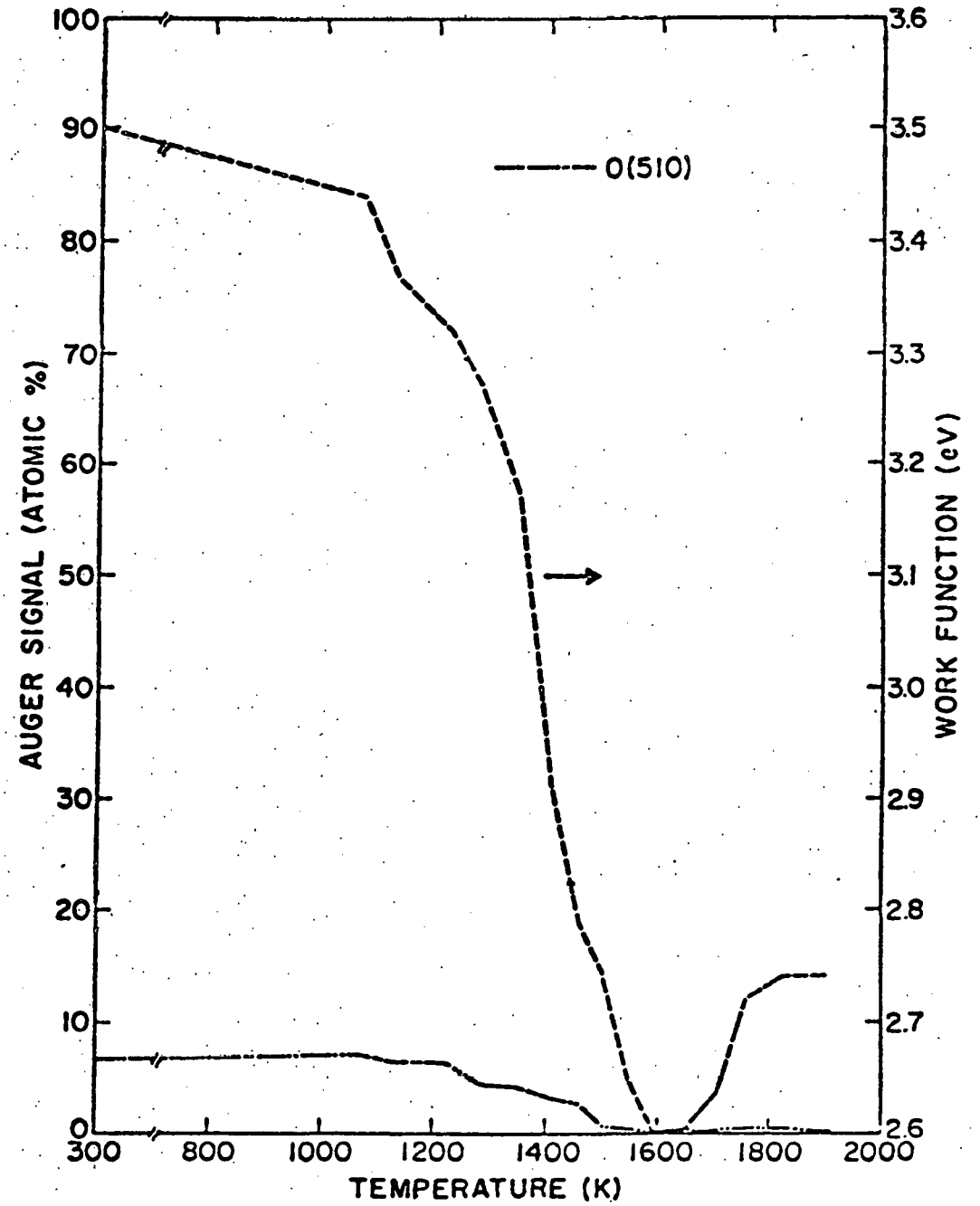

Figure 8. FERP work function and elemental AES signal vs heating temperature for MA-15 (110) with oxygen exposure at 300°K (Measurements by L. Swanson, Oregon Graduate Center, Beaverton, Oregon)

DISCUSSION

Chemical Analysis

The impurity content of the as-received hot pressed LaB_6 material varies significantly between 0.7 and 0.1 $^{w}/o$. Due to the significant purification of the zone refining technique, the metallic impurities were reduced to less than 30 ppm weight after only three zone passages of the hot pressed rods. Extreme purification resulted from even a single passage. This rapid purification was a result of the vaporization of impurities from the molten zone in addition to the normal zone refining action.

Takagi and Ishii (38) have also observed considerable purification of hot pressed LaB_6 by a laser-heated floating zone. (They also obtained their LaB_6 material from Cerac Incorporated.)

The major impurities remaining after three zone passages are carbon, tungsten, and the rare earths. The rare earths are not effectively removed by zone refining. This is probably due to the formation of the complete solid solution among the rare earth borides (39). Because of their high melting point and low vapor pressure, tungsten and carbon were not removed by vaporization as were some other elements. Instead, as the data of Tables 3 and 5 indicate, they were redistributed in the molten zone by equilibrium partitioning, the classical mode of zone refining.

The vacuum fusion analyses revealed no reduction in oxygen content after the initial zone passage. This would indicate that perhaps the

oxygen measured for the zone refined rods was mainly a surface oxide formed in the presence of air at room temperature, because several investigators (40,41,42) have reported that LaB_6 forms a thin oxide coating at room temperature. Hence, it appears likely that the majority of the oxygen was removed during the initial zone passage.

The wet chemical analyses clearly indicate that the stoichiometry of hot pressed and zone refined material of lot C is less than the theoretical 6.0 value. The melting temperatures measured with this material were lower than that reported for stoichiometric LaB_6, 2715°C (43). This supports the nonstoichiometric B/La ratio, approximately 5.75, calculated from the wet chemical analyses.

Comparison of the B/La ratio of the starting blanks of lots A, B, and C materials with the B/La ratio of their respective zone refined rods reveals that the first zone passage reduces the B/La ratio significantly. Additional zone passages do not have a large effect upon the B/La ratio. In order to explain this phenomenon one could postulate that the boron is evaporating faster than lanthanum on the first zone passage but not on subsequent zone passages. However, it seems likely that a preferential evaporation would continue after one zone pass unless a congruently vaporizing composition (CVC) was obtained. Storms' data argue against this latter possibility as he measures the CVC at B/La ratios of greater than 6.04 for $T > 1700°K$. A more plausible explanation of the drop in the B/La ratio on the first zone pass can be related to the presence of free carbon in the

starting LaB_6 blanks, as revealed by the presence of residue upon dissolution. This carbon is removed on the first zone pass and if it were to preferentially remove boron with it as some type of B-C compound, one could account for the drop in the B/La ratio on the first pass and not on subsequent passes.

Metallography

Some very small (0.1 by 2 μm) inclusions were occasionally observed in the single zoned crystals in this study. Other investigators (20,38) have observed a brass-colored inclusion in float zoned LaB_6. They believed these inclusions to be LaB_4. Takagi and Ishii (38) using wavelength dispersive electron microprobe analysis (EPMA) observed the inclusions to be composed of only lanthanum and boron. In the present study using energy dispersive EPMA, only lanthanum was detected within the inclusions observed in this study. (Boron cannot be detected with the energy dispersive detector.) Since X-ray powder diffraction patterns in the present work did not reveal any lines other than those due to LaB_6, it is possible the "inclusions" may be a polishing artifact. No conclusion can be made as to the origin of these inclusions.

Lattice Parameter Measurements

The lattice parameters measured in the present work (Table 11) agree well with previously published values given in Table 16, except for those of Post *et al.* (7). The value of Post *et al.* deviates from the other lattice parameters by more than the expected probable error.

(The maximum probable error expected would be $\pm$ 0.0007Å, based upon the results of the precision lattice parameter project (44).)

Johnson (5) observed that the lattice parameter of LaB_6 in equilibrium with LaB_4 and that of LaB_6 in equilibrium with boron were equal within an experimental error of $\pm$ 0.0003Å. Therefore, disagreement of the value of Post et al. cannot be attributed to a difference in the B/La ratio.

Referring to Table 11, it is apparent that the lattice parameter of MC-1-E correlates with a higher carbon content, thus indicating that the lower lattice parameter of MC-1-E might be caused by the presence of carbon. Post et al. obtained their LaB_6 by reaction of lanthanum and boron in a carbon crucible. Their LaB_6 contained a large amount of carbon, 0.1 to 0.5 $^w/_o$, and this could account for their smaller value of the lattice parameter. Bertaut and Blum (6), Swanson and Dickinson (45), and Schmidt et al. (46) obtained LaB_6 by a fused salt reaction and one would not expect a high carbon content. The lattice constants of MA-37 and MC-4-E could indicate a decrease in lattice parameter as the B/La ratio decreases from stoichiometry. However, if there is a change, it is less than 0.0003Å and the measurements were not of sufficient precision to allow this change to be established.

Density Measurements

The measured density and lattice parameter of the single crystals, ρ = 4.70 to 4.71 gm/cm^3 and a_o = 4.1567Å respectively, indicates a B/La ratio of near 6.0, whereas, the wet chemical analyses measure a

Table 16. Lattice constant of LaB_6

a_o (Å)	Investigator
4.153	Post et al. (7)
4.156	Swanson and Dickinson (45)
4.1561	Schmidt et al. (46)
4.1561	Johnson (5)
4.1566	Bertaut and Blum (6)
4.1567	MA-37 (this study)
4.1564	MC-4 (this study)

B/La ratio of approximately 5.75. There are two ways to analyze the data in order to understand this discrepancy.

First analysis

Storms and Mueller (47) have determined the phase boundary of LaB_4/LaB_6. The phase boundary composition was given as a B/La ratio of 6.014. If these results are correct, the crystals from lot C material must be assumed to be two-phase.

Because of the high purity, the second phase may be composed of only lanthanum and boron. The obvious choice for the second phase would be LaB_4. Johnson (5) measured the density of LaB_4 as 5.375 gm/cm^3. The average density, $\bar{\rho}$, of a mixture of LaB_4 and $LaB_{6.014}$ which has an overall B/La ratio 5.75, would be greater than 4.71 gm/cm^3. Thus, the "LaB_4" would have to be a defect compound. Furthermore, it would have to have lanthanum vacancies rather than boron vacancies to provide a mixture of LaB_6 plus "LaB_4" such that the average density $4.70 \leq \bar{\rho} \leq 4.71$ gm/cm^3 when B/La = 4.75. The composition of the "LaB_4" was calculated assuming:

(a) $LaB_{6.014}$ is really $La_{0.9978}B_{6.0}$

(b) $\rho(LaB_{6.014}) = 4.704$ gm/cm^3

(c) "LaB_4" is really $La_\chi B_{16}$

(d) Volume of "LaB_4" unit cell = 224.343A^{o3}

(e) R = B/La = 5.75

(f) $4.70 \leq \bar{\rho} \leq 4.71$.

Letting Y be mole fraction of "LaB_4", the mixture can be written as (1-Y) $La_{0.9978}B_6$ + Y ($La_\chi B_{16}$). Thus,

$$R = \frac{6 + 10Y}{.9978\ (1-Y) + \chi Y} \quad \text{or} \quad Y = \frac{6.0 - 0.9978R}{\chi R - 0.9978R - 10}$$

and $$\rho\ (\text{"}LaB_4\text{"}) = \frac{\chi(138.91) + 16(10.811)}{.60222 \times 224.343}$$

Therefore, $3.31 \leq \chi \leq 3.36$ and $0.080 \leq Y \leq 0.073$. These results indicate that "LaB_4" would be somewhere between $LaB_{4.76}$ and $LaB_{4.83}$, and the mole percent would be between 7.3 and 8%. When Y is converted from mole fraction to volume fraction, the analysis predicts a second phase volume fraction for "LaB_4" of around 20%. It seems likely that such large amounts of second phase would have been detected by the metallographic or X-ray analyses.

Second analysis

If the zone refined crystals of lot C material are assumed to be a single-phase material, then $LaB_{5.75}$ must be a defect structure, "LaB_6". Two possible defect structures would cause a decrease in B/La ratio, boron vacancies and lanthanum interstitials. The type of defect structure can be evaluated utilizing the following relationship:

$$\rho(\text{"}LaB_6\text{"}) = \frac{n_B A_B + n_{La}\ A_{La}}{N\ \ V} \qquad (12)$$

where n_B = number of boron atoms per unit cell

n_{La} = number of lanthanum atoms per unit cell

A_B = atomic weight of boron

A_{La} = atomic weight of boron

N = Avogadro's number

V = volume of the unit cell

$\rho(\text{"}LaB_6\text{"})$ = density of defect structure

Since the B/La ratio is 5.75, $n_B/n_{La} = 5.75$ by definition. If we assume lanthanum interstitial defects, then $n_B = 6.0$, $n_{La} = 1.043$, and $\rho(\text{"}LaB_6\text{"}) = 4.85$ gm/cm^3. If we assume boron vacancy defects, then $n_B = 5.75$, $n_{La} = 1.0$, and $\rho(\text{"}LaB_6\text{"}) = 4.649$ gm/cm^3. Since neither defect structure provides the proper density $4.70 \leq \rho(\text{"}LaB_6\text{"}) \leq 4.71$, it can be assumed that a simple interstitial or vacancy mechanism does not exist. However, a combination of both mechanisms could satisfy the density requirement. This may be thought of as follows. The loss of boron occurs by vacant boron octahedrons in the lattice and some of these vacant octahedral positions are filled by an additional lanthanum atom. Since the boron octahedron is composed of six boron atoms, the number of boron atoms per unit cell can be related to the number of vacant octahedrons per million unit cells, m, by $n_B = 6(\frac{10^6 - m}{10^6})$. Utilizing Equation 12, m is found to range between 29,200 and 31,100 for the respective values of $n_{La} = 1.013$ and 1.011 which provide 4.70 gm/cm^3 $\leq \rho(\text{"}LaB_6\text{"}) \leq$ 4.71 gm/cm^3. These results imply that approximately 3% of the unit cells are missing a boron octahedron, and that approximately 2 of every 5 boron octahedral voids are filled by a lanthanum atom. Although complex, this mechanism is feasible in terms of the electron requirements and in terms of spatial considerations.

Thermionic Properties

For comparative purposes the thermionic emission data of various researchers has been replotted in Figure 9. Also, the brightness measurements of MA-8, MC-9, MC-10, and MC-11 are included in Figure 9. The cathode current density was calculated using Equation 2 assuming a Langmuir efficiency of 100%.

Although there is considerable spread in these data, several groupings are noticed. These are indicated on the figure by lines 1 through 5. Referring to Equation 3, these lines may be identified by their Richardson emission constant, A, and apparent work function, ϕ, and are given in Table 17. There appears to be a correlation between the character of the LaB_6 used and the line about which the data are grouped. The data from Storms and Mueller (48) are grouped about line 2. Plotted are their data of sintered LaB_6 that had surface compositions with B/La equal to 6.02 and 6.03. From the chemical analysis given, their sintered LaB_6 is known to have a high oxygen content ($\sim$0.1 $^{w}/o$). Also grouped about line 2 are the data for a (100) single crystal measured by Oshima et al. (49). Even though their crystals were single pass float zone refined, they note segregation of carbon atoms from the interior of their crystals to the surface. Hence, the data grouped about line 2 are believed to be due to LaB_6 with high oxygen and/or high carbon content. The data about line 1 are those of Berrada et al. (42). No chemical analyses are given, however, since they are arc melted a high impurity content is probable.

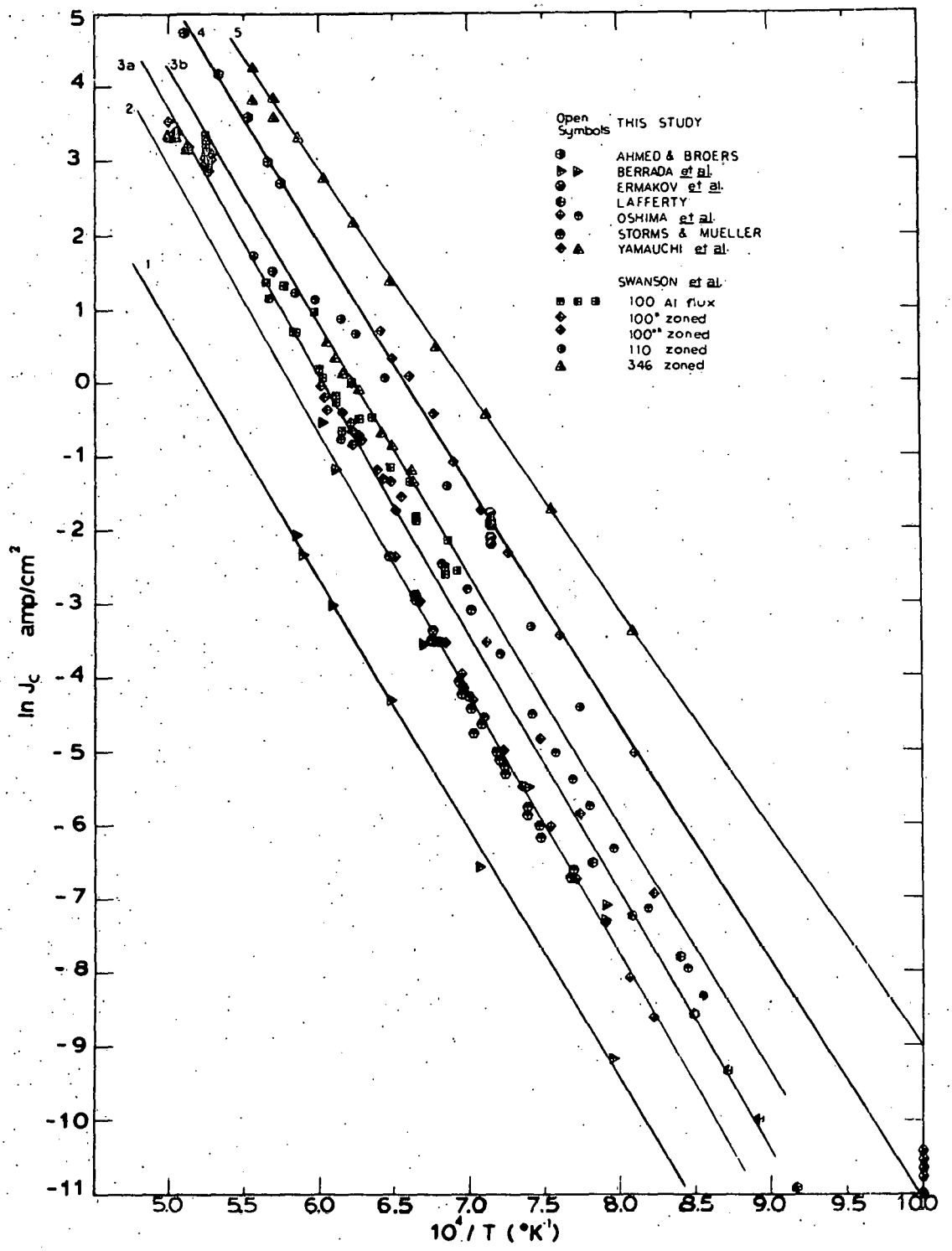

Figure 9. Various observed current densities for LaB_6

Table 17. Thermionic constants for figure lines

Line[a]	A (amp $^{o}K^{2}/cm^{2}$)	ϕ (eV)
1	2.9	2.67
2	55	2.81
3a	120	2.80
3b	120	2.70
4	120	2.55
5	74	2.34

[a]Lines 1, 2 and 5 are linear regressions. Lines 3a, 3b, and 4 are reference lines which correspond to the A and ϕ values shown.

In Figure 10, with the exception of the data of Ahmed and Broers (13), only data of known high purity (< 100 ppm) are shown. These data correspond to most of the data on Figure 9 falling about the upper lines 3, 4, and 5. Swanson and Dickinson (45) state the bulk impurities in their aluminum flux grown crystals to be less than 100 ppm. The crystals used by Yamauchi et al. (25) are those prepared by Takagi and Ishii (38), and the impurities in the LaB_6 used by Yamauchi et al. are stated to be less than 100 ppm. The majority of the data, as seen in Figure 10, are scattered between lines 3a and 3b. The source of these data are Yamauchi et al. (25), Swanson and Dickinson (45), Swanson et al. (50), Figure 7c and the 100^* data for MA-20. The data near line 4 are the data from Ahmed and Broers (13) and the 100^{**} data for MA-20.

It is interesting to point out the (100) crystal, MA-20, analyzed by Swanson displayed a dependence of work function upon thermal treatment as shown on Figure 7b. A heat treatment produced a significant lowering of the work function (from 100^* to 100^{**} on the figure). The cause of the work function change is unknown. Swanson (45,50) has also measured the thermionic emission of (100) crystals grown by the aluminum flux method. Although heat treated similarly, the thermionic emission obtained from these crystals is significantly lower than that for MA-20, 100^{**}. (See Figure 10.) Two possible explanations as to the difference are:

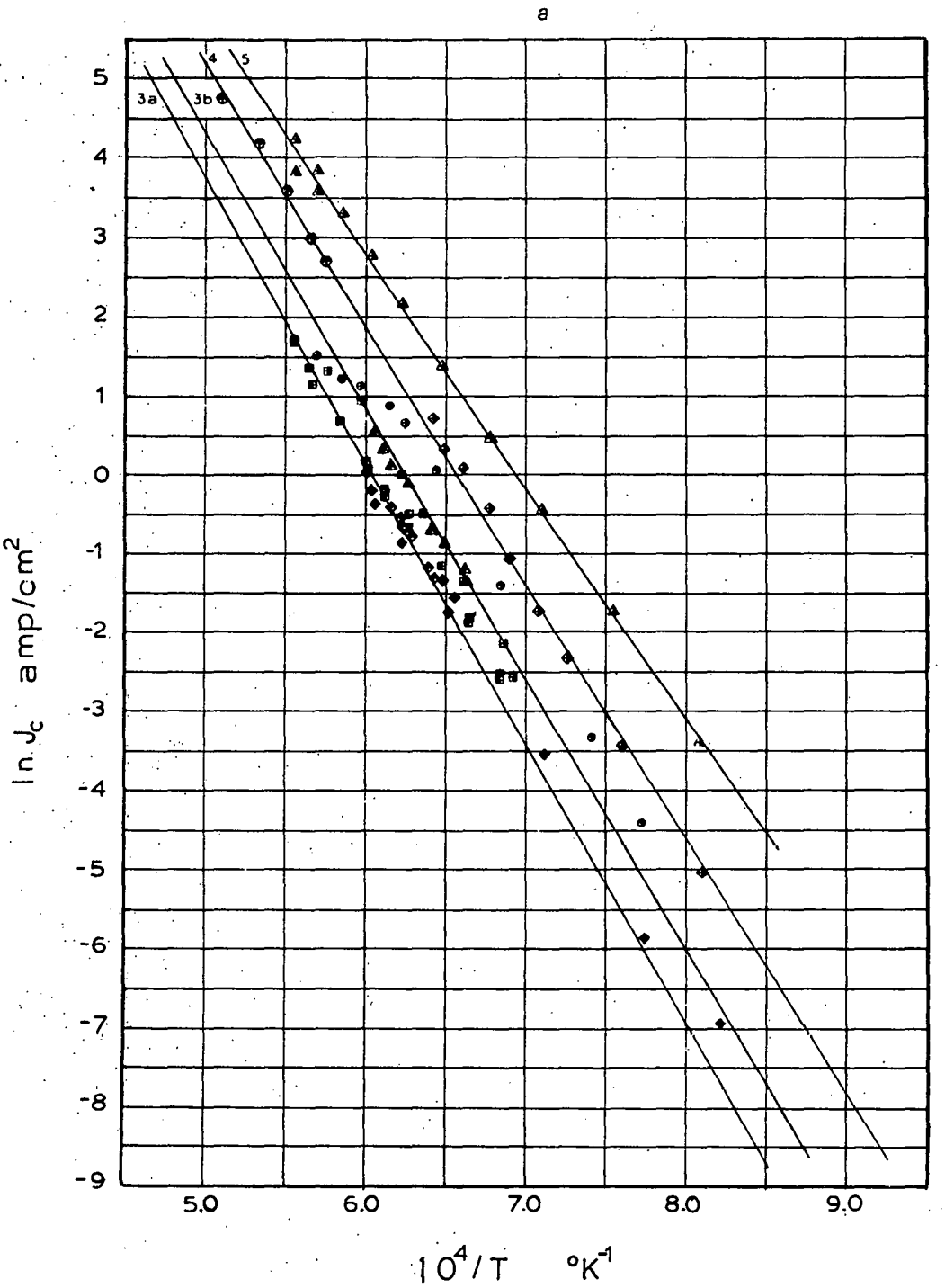

Figure 10. Current densities of high purity LaB_6

(a) Aluminum flux crystals may have a higher oxygen content and hence are self-poisoning. That is, the increased emission is due to a cleaner surface.

(b) Aluminum flux crystals probably have a higher B/La ratio (near 6.0) and this may result in a higher work function.

Swanson has measured the emission as a function of oxygen desorption on crystal MA-15. These results shown in Figure 8 show the emission to be very sensitive to surface oxygen content and support explanation (a) above.

Jacobson and Storms (51) measured the thermionic emission for lanthanum-boron compounds. The thermionic emission of sintered samples $LaB_{8.5}$ and $LaB_{6.01}$ measured at a temperature of 1400°K are 0.0046 and 0.011 amp/cm^2, respectively. Recent data were obtained from Storms and Mueller (48). Their data show a steady decrease in thermionic emission as the B/La ratio increases and support explanation (b). Thus, either or both explanations, (a) and (b), may be the cause of the higher thermionic emission.

LaB_6 Evaporation

The mass loss rates, (gm/cm^2·sec), measured in this study are shown on Figure 11. The data of Storms and Mueller (47) are also plotted on the figure. It may be seen that there is reasonably good agreement with their data. The right-hand axis is given as a radial loss rate, $\Delta\dot{r}$ (μm/hr). This scale is useful in estimating cathode lifetimes.

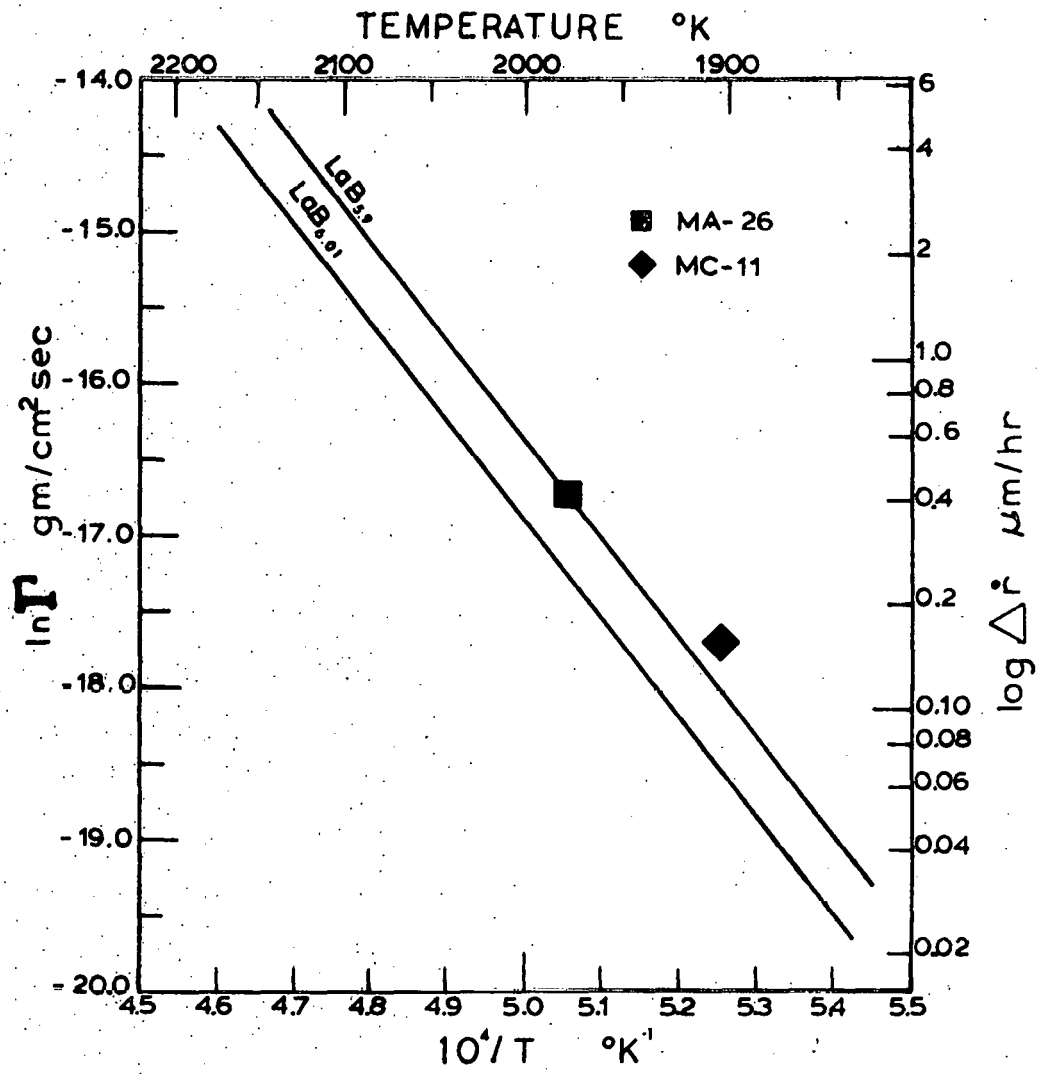

Figure 11. LaB_6 evaporation rate curves for LaB_6 with B/La ratios of 6.01 and 5.9

Brightness

A useful figure for those utilizing LaB_6 as a cathode material in electron microscopes would be one showing brightness, B (amp/cm^2·steradian), as a function of cathode lifetime, rather than one showing current density versus temperature, as in Figures 9 and 10. Such a figure (Figure 12) was constructed using Equation 2 and a Langmuir efficiency of 100% to convert current density to theoretical brightness at 20 kV. The lines 2 through 4 on Figure 12 were converted from the lines labelled 2 through 4 on Figure 10. The equation of Storms and Mueller (47) for the mass loss rate of LaB_6 was used to calculate a change in radius per hour, $\Delta\dot{r}$, due to vaporization of material. The brightness measured for ion pumped systems, Ferris et al. (52), Nakagawa and Yanaka (53), Broers (54) and this study fall between lines 3a and 3b. It is concluded that to obtain the maximum brightness from LaB_6 cathodes at lifetimes greater than 500 hours (1 mm diameter cathode) a number of variables must be controlled.

(a) The electron gun must be properly aligned and high bias voltages are necessary to prevent space charge limitation.

(b) The cathode must be thermally cleaned at temperature greater than 1650°K.

(c) LaB_6 of low impurity content must be used. This can be obtained by float zone refining. For most starting concentrations a single pass will reduce impurity content

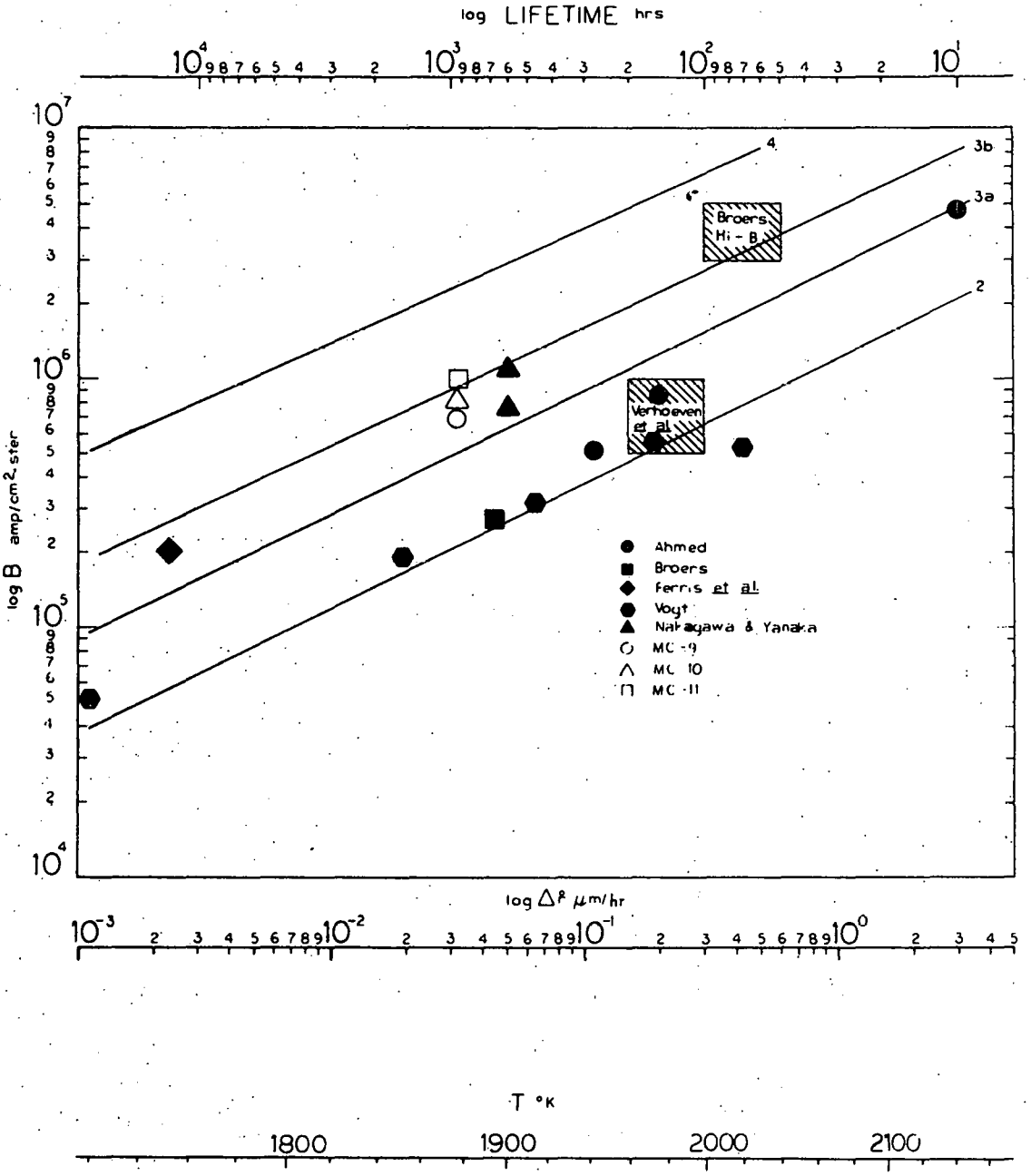

Figure 12. Brightness of LaB_6 cathodes vs evaporation rate

to acceptable levels and three passes will reduce impurities to less than 0.003 $^{w}/_{o}$.

(d) The residual pressure of oxygen must be reduced to extremely low values. Partial pressure of oxygen should be on the order of 10^{-10} mmHg. This can be achieved by an ion pumped gun chamber at pressures less than 1×10^{-6} mmHg.

When the above conditions are met, it is possible to operate a 1 mm LaB_6 cathode at 20 kV with a brightness of 10^6 amp/cm^2·steradian and a lifetime of greater than 500 hours at a tip temperature of ~1900^{o}K.

LITERATURE CITED[y]

1. D. B. Langmuir, Proc. Inst. Rad. Eng., 25, 977 (1937).

2. J. M. Lafferty, J. Appl. Phys., 22, 299 (1951).

3. F. W. Heemstra, "Thermionic Work Functions of Some Rare Earth Borides," Masters Thesis, Iowa State University, Iowa, 1953.

4. R. W. Decker and D. W. Stebbins, J. Appl. Phys., 26, 1004 (1955).

5. R. W. Johnson, "The Lanthanum-Boron System," Masters Thesis, Iowa State University, Iowa, 1959; J. Phys. Chem., 65, 909 (1961).

6. F. Bertaut and P. Blum, Comp. Rend., 234, 2621 (1952).

7. B. Post, D. Moskowitz, and F. W. Glaser, J. Am. Chem. Soc., 78, 1800 (1956).

8. A. N. Broers, J. Appl. Phys., 38, 1991 (1967).

9. A. N. Broers, J. Phys. E: Sci. Instrum., 2, 273 (1969).

10. H. Ahmed, in "5th European Congress on Electron Microscopy, University of Manchester, 1972," P. W. Hawkes, Ed., The Institute of Physics, London, 1973, p. 10.

11. J. D. Verhoeven and E. D. Gibson, J. Phys. E: Sci. Instrum., 9, 65 (1976).

12. R. Vogt, Optik, 36, 262 (1972).

13. H. Ahmed and A. N. Broers, J. Appl. Phys., 43, 2185 (1972).

14. V. S. Fomenko, "Handbook of Thermionic Properties," Plenum Press Data Division, New York, 1966, p. 88.

15. G. V. Samsonov, "High Temperature Compounds of Rare Earth Metals and Nonmetals," Consultants Bureau, New York, 1965, p. 26.

16. S. V. Ermakov, F. G. Mamedov, G. A. Meerson, and B. M. Tsarev, Neorg. Mater., 3, 808 (1967).

17. A. N. Broers, in "Scanning Electron Microscopy/1975," O. Johari and I. Corvin, Eds., IIT Research Institute, Chicago, 1975, p. 662.

18. N. G. Pfann, "Zone Melting," John Wiley and Sons, Inc., New York, 1959, p. 23.

19. R. W. Johnson, J. Appl. Phys., 34, 352 (1963).

20. E. F. Westrum, Jr., H. L. Clever, J. T. S. Andrews, and G. Feick, in "Proceedings of the Fourth Conference on Rare Earth Research," L. Eyring, Ed., Gordon and Breach Science Publishers, New York, 1964, p. 597.

21. T. Tanaka, E. Bannai, S. Kawai, and Y. Yamane, J. Cryst. Growth, 30, 193 (1975).

22. G. V. Samsonov, "High-Temperature Compounds of Rare Earth Metals with Nonmetals," Consultants Bureau, New York, 1965, p. 45.

23. J. D. Verhoeven, E. D. Gibson, M. A. Noack, and R. J. Conzemius, J. Cryst. Growth, 36, 115 (1976).

24. F. A. Schmidt, R. J. Conzemius, O. N. Carlson, and H. J. Suec, Anal. Chem., 46, 810 (1974).

25. H. Yamauchi, K. Takagi, I. Yuito, and U. Kawabe, Phys. Lett., 29, 638 (1976).

26. L. W. Swanson, J. T. Dickinson, and D. R. McNeely, "Fabrication and Surface Characterization of Composite Refractory Compounds Suitable for Thermionic Converters," NASA Contractor Report 2668, Washington, D. C., 1976.

27. A. Smakula and V. Sils, Phys. Rev., 99, 1744 (1955).

28. G. A. Bell, Australian J. Appl. Sci., 9, 236 (1958).

29. A. Smakula, in "Methods of Experimental Physics," K. Lark-Horovitz, Ed., Academic Press, New York, 1959, Volume 6A, p. 283.

30. L. W. Tilton and J. K. Taylor, J. Res. NBS, 18, 213 (1937).

31. R. C. Weast, Ed., "Handbook of Chemistry and Physics," 51st edition, The Chemical Rubber Company, Cleveland, 1970, p. F-1.

32. J. D. Verhoeven and E. D. Gibson, in "Scanning Electron Microscopy/1977," O. Johari, Ed., IIT Research Institute, Chicago, 1977, p. 9.

33. A. N. Broers, in "Scanning Electron Microscopy/1974," O. Johari and I. Corvin, Eds., IIT Research Institute, Chicago, 1974, p. 9.

34. C. J. Smithells, "Metals Reference Book," Butterworths, Washington, D. C., 1962, Volume II, p. 724.

35. R. C. Weast, Ed., "Handbook of Chemistry and Physics," 51st edition, The Chemical Rubber Company, Cleveland, 1970, p. D-137.

36. J. A. Bearden, Rev. Mod. Phys., 39, 78 (1967).

37. R. W. Strayer, W. Mackie, and L. W. Swanson, Surf. Sci., 34, 225 (1973).

38. K. Takagi and M. Ishii, J. Cryst. Growth, 40, 1 (1977).

39. P. Stecher, A. Neckel, F. Benesovsky, and H. Nowotny, Planseeber. Pulvermetallurgie, 13, 37 (1965).

40. B. Goldstein and D. J. Szostak, Surf. Sci., 74, 461 (1978).

41. A. Berrada, J. P. Mercurio, and J. Etourneau, Surf. Sci., 72, 177 (1978).

42. A. Berrada, J. P. Mercurio, J. Etourneau, and P. Hagenmuller, J. Less-Common Metals, 59, 7 (1978).

43. O. A. Mordovin and E. N. Timofeeva, Zhur. Neorg. Khim., 13, 3155 (1968).

44. W. Parrish, Acta Cryst., 13, 838 (1960).

45. L. W. Swanson and T. Dickinson, Appl. Phys. Lett., 28, 578 (1976).

46. P. H. Schmidt, L. D. Longinotti, D. C. Joy, S. D. Ferris, and H. J. Leamy, J. Vac. Sci. Technol., 15, 1554 (1978).

47. E. Storms and B. Mueller, J. Phys. Chem., 82, 51 (1978).

48. E. Storms and B. Mueller, unpublished research, Los Alamos Scientific Lab., Los Alamos, New Mexico, 1979.

49. C. Oshima, E. Bannai, T. Tanaka, and S. Kawai, J. Appl. Phys., 48, 3925 (1977).

50. L. W. Swanson, M. Gesley, and D. R. McNeely, "Fabrication and Surface Characterization of Composite Refractory Compounds Suitable for Thermionic Converters," NASA Interim Report #2, Oregon Graduate Center, Beaverton, 1977.

51. D. L. Jacobson and E. K. Storms, IEE Trans. Plasma Sci., PS-6, 191 (1978).

52. S. D. Ferris, D. C. Joy, H. J. Leamy, and C. K. Crawford, in "Scanning Electron Microscopy/1975," O. Johari and I. Corvin, Eds., IIT Research Institute, Chicago, 1975, p. 11.

53. S. Nakagawa and T. Yanaka, in "Scanning Electron Microscopy/1975," O. Johari and I. Corvin, Eds., IIT Research Institute, Chicago, 1975, p. 19.

54. A. N. Broers, J. Vac. Sci. Technol., 10, 979 (1973).

55. W. J. Schuele, J. F. Hazel, and W. M. McNabb, Anal. Chem., 28, 505 (1956).

56. L. N. Kugai and T. N. Nazarchuk, Zhur. Anal. Khim., 16, 205 (1961).

57. J. W. Tereshko, Anal. Chem., 35, 157 (1963).

ACKNOWLEDGMENTS

I wish to thank those who have made this investigation stimulating, rewarding, and a reality. To my major professor, Dr. John D. Verhoeven, I express my appreciation for his encouragement and advice. To Mr. E. D. Gibson, whose suggestions and instruction of the SEM were of considerable value, I extend my warmest thanks. And to my wife, Jeanne, I am deeply grateful for her patience and support without which my goals would not have been achieved.

APPENDIX: PROCEDURE FOR ANALYSIS OF LANTHANUM AND BORON

An analytical procedure similar to that recommended for hexaborides (55,56) was used to obtain lanthanum and boron concentrations. Samples were dissolved in a Parr acid digestion bomb with a 25 ml Teflon cup containing 6 ml of 1:1 HNO_3. Heating the bomb to 110°C for ten minutes resulted in the dissolution of the sample. After cooling, the solution was poured into a 100 ml volumetric flask and distilled water was used to bring it to volume. A 25 ml aliquot was titrated with approximately 0.05 M EDTA using a 10 ml buret to determine the lanthanum concentration. For the boron concentration, a 15 ml aliquot was titrated using a 10 ml buret according to the procedure of Tereshko (57) with approximately 0.1 M NaOH. Additional mannitol was added to the solution and was back-titrated until a stable pH = 8.20 $\pm$ 0.05 was maintained. All titration readings were estimated to the nearest one-hundredth of a milliliter.

An estimate of the reproducibility of the lanthanum-boron determination was obtained from the analysis of #1155 LaB_6 powder. This powder was purchased from Cerac Incorporated. Their literature stated this powder was the grade used in manufacturing hot pressed LaB_6 blocks. Two 100 mg portions were taken from the one pound lot. Each portion was dissolved separately. Two titrations for each element were performed on each solution.